International Journal of
Molecular Sciences

MDPI

Article

Evaluation of In Vitro Distribution and Plasma Protein Binding of Selected Antiviral Drugs (Favipiravir, Molnupiravir and Imatinib) against SARS-CoV-2

Orsolya Dömötör * and Éva A. Enyedy

MTA-SZTE Lendület Functional Metal Complexes Research Group, Department of Inorganic and Analytical Chemistry, Interdisciplinary Excellence Centre, University of Szeged, Dóm tér 7, H-6720 Szeged, Hungary
* Correspondence: domotor.o@chem.u-szeged.hu

Abstract: There are a number of uncertainties regarding plasma protein binding and blood distribution of the active drugs favipiravir (FAVI), molnupiravir (MOLNU) and imatinib (IMA), which were recently proposed as therapeutics for the treatment of COVID-19 disease. Therefore, proton dissociation processes, solubility, lipophilicity, and serum protein binding of these three substances were investigated in detail. The drugs display various degrees of lipophilicity at gastric (pH 2.0) and blood pH (pH 7.4). The determined pK_a values explain well the changes in lipophilic character of the respective compounds. The serum protein binding was studied by membrane ultrafiltration, frontal analysis capillary electrophoresis, steady-state fluorometry, and fluorescence anisotropy techniques. The studies revealed that the ester bond in MOLNU is hydrolyzed by protein constituents of blood serum. Molnupiravir and its hydrolyzed form do not bind considerably to blood proteins. Likewise, FAVI does not bind to human serum albumin (HSA) and α1-acid glycoprotein (AGP) and shows relatively weak binding to the protein fraction of whole blood serum. Imatinib binds to AGP with high affinity (logK' = 5.8–6.0), while its binding to HSA is much weaker (log$K' \leq$ 4.0). The computed constants were used to model the distribution of IMA in blood plasma under physiological and 'acute-phase' conditions as well.

Keywords: tyrosine kinase inhibitor; COVID-19; proton dissociation; lipophilicity; plasma protein binding; binding constants

Citation: Dömötör, O.; Enyedy, É.A. Evaluation of In Vitro Distribution and Plasma Protein Binding of Selected Antiviral Drugs (Favipiravir, Molnupiravir and Imatinib) against SARS-CoV-2. *Int. J. Mol. Sci.* **2023**, *24*, 2849. https://doi.org/10.3390/ijms24032849

Academic Editors: Jacek Z. Kubiak and Malgorzata Kloc

Received: 8 December 2022
Revised: 17 January 2023
Accepted: 29 January 2023
Published: 2 February 2023

1. Introduction

The outbreak of the COVID-19 pandemic in the first months of 2020 posed a serious challenge for medical establishments worldwide. Rapid spread and the unpredictable outcome of the infection required the urgent development of effective drug therapies to prevent the progression of severe illness and to stop transmission of SARS-CoV-2. In this respect, off-label use of drugs previously approved for other illnesses emerged as a key strategy in the fight against the virus. Instead of the slow and costly development and approval of novel drugs, physicians started the clinical testing of antiviral agents originally developed against other types of RNA viruses like hepatitis C, HIV, or influenza. Remdesivir, ribavirin, lopinavir, favipiravir (FAVI), and molnupiravir (MOLNU) have been used to treat mild to severe COVID-19 cases in several countries based on such considerations [1–4]. Both FAVI and MOLNU (Scheme 1) are nucleoside analog prodrugs that were originally designed for treatment of influenza disease; FAVI was approved for this application in Japan in this indication [5–7]. Favipiravir is metabolized in cells to an active form, favipiravir-ribofuranosyl-5′-triphosphate, and inhibits viral RNA polymerase [6]. Molnupiravir acts in a slightly different way, namely, the isobutyrate function is hydrolyzed during absorption to form N(4)-hydroxycytidine (EIDD-1931), which is then triphosphorylated at the 5′-end in the cellular environment and promotes mutations in viral RNA

replication [1,8–10]. Favipiravir was authorized for treatment of COVID-19 in Japan, Russia, Serbia, Turkey, India, Egypt, and Hungary etc. under emergency provisions, while MOLNU was authorized in the US, UK, Bangladesh, and Israel. In addition to antiviral agents, drugs that modulate the extreme immune response triggered by infection have attracted attention as well. This group includes, among others, corticosteroids, interferon-1, thalidomide, (hydroxy)chloroquine and various cytokine and kinase inhibitors [3,4]. In this regard, the tyrosine kinase inhibitor (TKI) imatinib (IMA) (Scheme 1), originally designed for the treatment of chronic myeloid leukaemia (CML), has also been proposed as a potential therapy for COVID-19 disease [11,12]. In CML patients treated with TKIs, extremely low incidence of COVID-19 infection was reported, and in vitro data revealed that IMA as a Bcr-Abl tyrosine kinase inhibitor may block viral replication in the early stages of infection [11,13]. The immunomodulatory effect of IMA was also claimed to be capable of reducing severe inflammatory response [12].

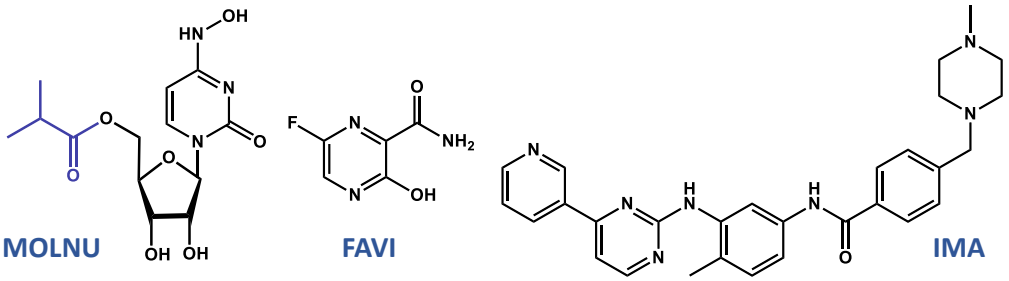

Scheme 1. Structure of the studied compounds molnupiravir (MOLNU), favipiravir (FAVI) and imatinib (IMA). Note: by hydrolysis of the ester group (blue) in MOLNU, isobutyric acid and N(4)-hydroxycytidine (EIDD-1931) are formed which together are referred as hydrolyzed molnupiravir (h-MOLNU) in this work.

All three medicines are delivered orally, otherwise their pharmacokinetic behavior differs significantly. Simple physicochemical features such as solubility, charge, and lipophilicity, as well as plasma protein binding are extremely important in terms of drug absorption, distribution, elimination, toxicity, and efficacy. Interestingly, there is little information available on these qualities in the cases of FAVI and MOLNU, and predicted data found in the common databases (DrugBank, PubChem) are often contradicting [14–17]. The product monograph for Avigan® (FAVI) reports good aqueous solubility and 54% serum protein binding of the drug observed in vitro [14]. This in vitro protein binding data appears to be referred to in the literature [17–21] as an in vivo result [17–21]. The fluorescence of FAVI was reported only recently in 2021 by S.M. Megahed et al. [22]. At the same time, several case reports on the fluorescence of nails, hair, skin, face, and sclera of patients were published by Turkish clinicians after treatment with FAVI, although this phenomenon was associated with the active ingredient in only one publication, using Wood's light for examination of patients and the halved tablets [23–25]. No plasma protein binding was observed for EIDD-1931 in vitro, and no such data is available for MOLNU [15]. The interaction of IMA with human serum albumin (HSA) and α1-acid glycoprotein (orosomucoid, AGP) has been reported in the literature, but the role of these two proteins has not been clearly elucidated yet [26–33]. Both HSA and AGP are acute phase proteins (APP), namely their concentrations change considerably in the blood in response to inflammation. The serum concentration of AGP increases two- to three-fold during acute phase response (positive APP), whereas HSA concentration decreases during inflammation (negative APP) [34–36]. The orosomucoid AGP is the second most important transport protein for organic drugs in blood, next to HSA. At the same time, physiological concentration of AGP is much lower (approximately 10–20 μM) in comparison to albumin (ca. 630 μM) [36,37]. Therefore, serum protein binding of IMA can be severely affected by inflammation, which is a possible consequence of viral infections or tumor diseases [32,38,39]. Neutral or negatively charged drugs bind primarily to HSA, while drugs possessing basic functional groups tend to show

affinity for AGP [36,37,40]. Taking this observation into account, different protein binding preferences are expected for FAVI, MOLNU and IMA in blood plasma.

The three orally administered heterocyclic aromatic drugs with dissociable moieties, FAVI, MOLNU and IMA, were selected here for detailed in vitro blood distribution studies. The available literature on these compounds' protonation processes, lipophilicity, thermodynamic aqueous solubility, and blood serum protein binding is fairly limited. Our goal was to provide a comprehensive overview of these properties as well as to critically examine the literature data and potential shortcomings of the approaches used in this work. The proton dissociation processes were monitored by pH-potentiometry, UV–visible and fluorescence spectroscopies, and/or by *n*-octanol/water partition experiments also considering the solubility and stability issues of the compounds under investigation. The interaction of the compounds with whole blood serum, and the binding to serum proteins HSA and AGP was investigated as well. Results on the protein binding were obtained using a combination of separation techniques such as membrane ultrafiltration and frontal analysis capillary electrophoresis (FACE), as well as spectroscopic methods, ^{1}H NMR spectroscopy, steady-state fluorometry and fluorescence anisotropy.

2. Results and Discussion

2.1. Aqueous Stability and Solubility

Molnupiravir, one of the title compounds, contains an ester functional group that may hydrolyze under certain conditions. Therefore, the aqueous stability of MOLNU was investigated as a first step at pH 2.0, 7.4, and 12.0 by ^{1}H NMR spectroscopy. The NMR spectra (Figure 1) show that MOLNU hydrolyzes completely within 30 min at pH 12.0 resulting in isobutyrate and N(4)-hydroxycytidine (EIDD-1931). This process is much slower at pH both 2.0 and 7.4 than at pH 12; and in 5 days only 8% and 2% hydrolyzed products, respectively, were obtained. Deamination, which is characteristic for cytidine under alkaline and acidic conditions, was not observed probably due to the replacement of amine by a hydroxylamine group in the molecule [41,42]. The other two compounds, FAVI and IMA were stable in aqueous media at pH 2 and 7.4 at least for 30 h (Figures S1 and S2).

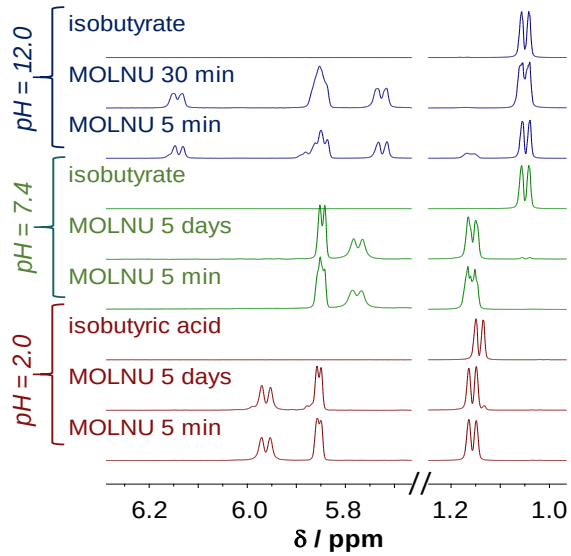

Figure 1. ^{1}H NMR spectra of MOLNU followed in time (5 min, 30 min, and 5 days) at pH 2.0, 7.4, and 12.0, corresponding spectra of isobutyric acid/isobutyrate are shown as well for comparison [c_{MOLNU} = 1 mM; 10% (*v*/*v*) D_2O/H_2O; *t* = 25 °C].

The studied compounds (Scheme 1) display different thermodynamic solubility (*S*) at various pH values and temperatures. Favipiravir and MOLNU exhibit excellent solubility (10 mM solutions could be prepared) at pH 2.0 and 7.4, both at 25 °C and 37 °C, while the solubility of IMA decreases with increasing pH and temperature (Figure 2). As a result of

the gradual deprotonation of the charged groups, the good solubility attained at pH 2.0 (S > 10 mM) declines to 14 µM by pH 8.2 (t = 37 °C), where the neutral form predominates (vide infra).

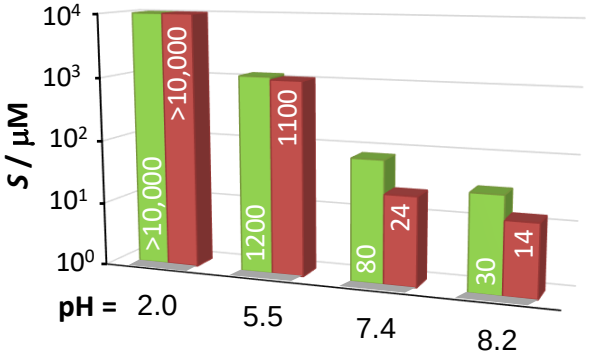

Figure 2. Thermodynamic solubility (S) of IMA at various pH values at 25 °C (green) and 37 °C (red), determined by UV-vis spectrophotometry [buffering solutions: 0.01 M HCl (pH = 2.0), 20 mM MES (pH = 5.5), 20 mM HEPES (pH = 7.4 and 8.2)].

2.2. Proton Dissociation Processes

Table 1 summarizes the proton dissociation constants (pKa) measured using pH-potentiometric, UV-visible (UV-vis) spectroscopic, and fluorometric titrations. *n*-Octanol/water partition experiments were used as well in the case of IMA and FAVI to obtain pK_a values.

One pK_a value could be determined for FAVI by various techniques which were in good agreement with each other. The *n*-octanol/water distribution coefficients (D_{pH}) obtained at various pH values reveal the more hydrophilic character of the deprotonated form (Figure 3), as deprotonation of the 3-hydroxy-pyrazine ring results in a negatively charged ion. In solution, FAVI can exist in keto-enol tautomeric forms, although the enol form was reported to be more stable in aqueous solution [43], thus the proton is likely to dissociate from the enol group or the iminol/amide group (Figure S3). Interestingly, based on theoretical calculations only protonation of the neutral molecule was taken into account, and proton dissociation was not investigated [43,44]. As a result of deprotonation, the weak fluorescence intensity of FAVI increases about ten-fold and bathochromic shift in the UV-vis absorption spectrum occurs as well (Figure 4 and Figure S3). This spectral shift is indicative of the formation of a more extended π-conjugated system suggesting the formation of the enolate tautomer upon deprotonation (Figure S3).

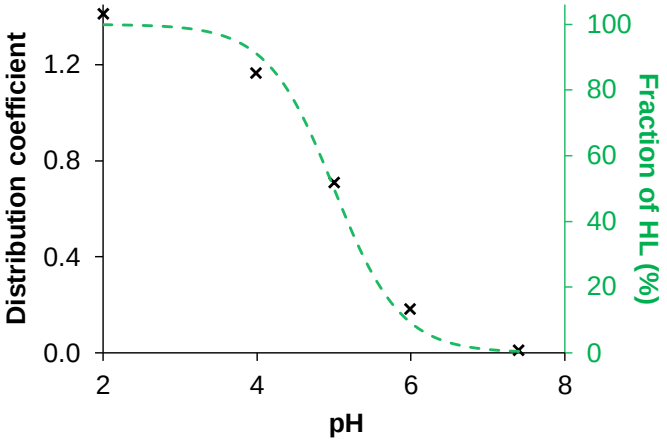

Figure 3. Distribution coefficient (D) of FAVI determined in *n*-octanol/aqueous systems at various pH values plotted together with the calculated molar fraction of the neutral HL form [ionic strength (I) = 0.1 M (KCl); t = 25 °C].

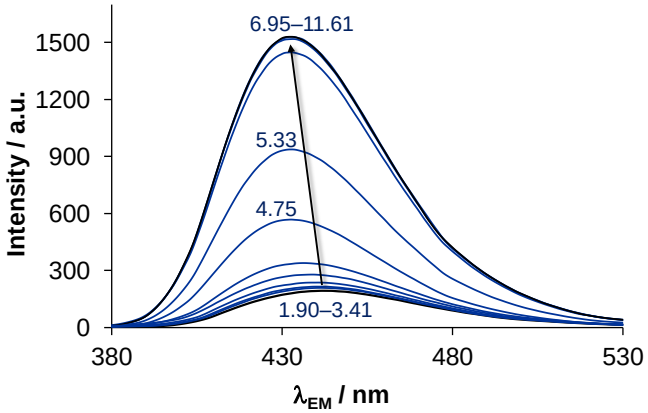

Figure 4. Fluorescence emission spectra of FAVI recorded at various pH values [c_{FAVI} = 5.0 μM; λ_{EX} = 360 nm; I = 0.1 M (KCl); t = 25 °C].

Two pK_a values could be determined for MOLNU by pH-potentiometric and spectrophotometric titrations, which belong to the N(4)-hydroxycytosine moiety. The UV-vis spectra in Figure 5 show characteristic changes between pH 2.0–4.0 and 9.5–11.5, which are not sensitive to the hydrolysis of the ester function. Repeated pH-potentiometric titration of the hydrolyzed MOLNU resulted in the appearance of an additional pK_a = 4.54 ± 0.08, that corresponds to the reported pK_a of isobutyric acid (pK_a = 4.67, I = 0.1 M $NaNO_3$) [45], while the original pK_a values were barely affected (see titration curves in Figure S4). The fully protonated form is positively charged (H_2L^+), and the molecule becomes neutral by the first proton dissociation process. Given the trend of lipophilicity data determined at pH 2.0 and 7.4, the zwitterionic character of this molecule is not plausible (vide infra). The second deprotonation occurs in the alkaline pH range (pK_a = 10.18 ± 0.02 determined by pH-potentiometry). The widely studied analogue, cytidine is characterized by one pK_a = 4.1–4.5 [46,47] assigned to the N(3)H^+ group. The pK_{a1} = 2.14 ± 0.01 of MOLNU is assumed to belong to the same group. The second deprotonation possibly takes place on the hydroxyamino/hydroxyimino functional group. The constants determined are in good agreement with the data in the product assessment report of the European Medicines Agency (pK_{a1} = 2.2, pK_{a2} = 10.2), however the existence of a third deprotonation, found in the same report (pK_{a3} = 12) [15], was not observed by us in the studied pH range.

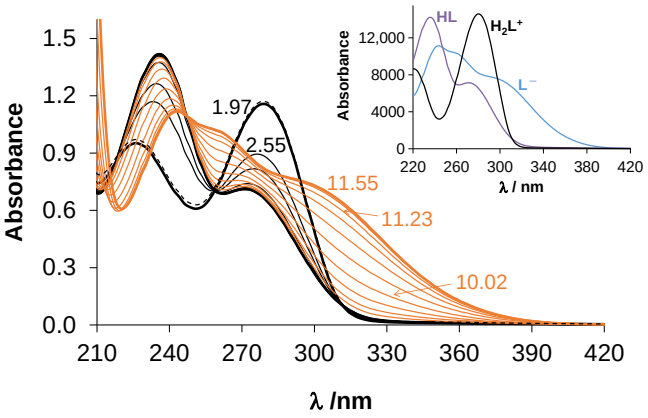

Figure 5. Absorbance spectra of MOLNU recorded in the pH range between 1.97 and 11.55 (solid lines) and after back-acidification at pH 1.97 (dotted line), inset shows computed individual molar spectra of the compound in different protonation states [c_{MOLNU} = 40 μM; I = 0.1 M (KCl), t = 25 °C].

Imatinib possesses four basic groups which can be protonated (Scheme 1, Table 1). The lowest pK_a determined by UV-vis titration corresponds to the secondary ammonium group. This value, together with pK_{a2} and pK_{a3} determined by pH-potentiometric titrations, agrees very well with the reported data of Szakács et al. (I = 0.15 M NaCl) [48]. The latter

two are macroscopic constants belonging to the pyridinium and one of the piperazinium nitrogens. Imatinib becomes neutral by dissociation of the last proton from the remaining piperazinium group and its solubility drops to the low-micromolar range (see Figure 2), making pH-potentiometric determination difficult. Additionally, this process is not associated with any spectral change in the UV-vis spectrum. Therefore, *n*-octanol/water distribution coefficients were determined at various pH values (Figure S5) and $pK_{a4} = 7.9 \pm 0.1$ could be computed, which is two tenths higher than the value reported by Szakács et al. (determined by pH-potentiometry using the titration curve until no precipitation occurred). Given the uncertainty of both methods, the agreement of these constants is acceptable.

The knowledge of these dissociation constants allowed us to compute fractions of the actual protonation states at various pH values (Figure S6) including pH 7.4 (pH of extra- and intracellular space) and pH 2.0 (a typical gastric pH) (Table 1). At pH 7.4, MOLNU has the neutral HL form, whereas FAVI is entirely deprotonated (L-), and IMA is mostly positively charged, with just around 25% neutral form. On the other hand, at pH 2.0 the protonated forms H_4L^{4+} and H_3L^{3+} predominate for IMA, FAVI is neutral (100% HL), whereas 58% and 42% of MOLNU are present in H_2L^+ and HL forms, respectively.

Table 1. Proton dissociation constants (pK_a) of the studied compounds determined by pH-potentiometry (pHm) UV-vis, fluorometry (fluor) or *n*-octanol/water partition (o/w part.), *n*-octanol/water distribution coefficients ($\log D_{pH}$), and calculated distribution (%) of the species in different protonation states at pH 7.40 and 2.0 [I = 0.1 M (KCl); t = 25 °C].

	IMA	**FAVI**	**MOLNU**
Proton dissociation processes			
	pK_{a1} 1.72 ± 0.01 (UV-vis) pK_{a2} 3.06 ± 0.05 (pHm) pK_{a3} 3.86 ± 0.03 (pHm) pK_{a4} >7.0 (pHm) 7.9 ± 0.1 (o/w part.)	pK_{a1} 5.11 ± 0.01 (pHm) 5.08 ± 0.01 (UV-vis) 5.17 ± 0.01 (fluor) 5.1 ± 0.1 (o/w part.)	pK_{a1} 2.14 ± 0.01 (pHm) 2.11 ± 0.01 (UV-vis) pK_{a2} 10.18 ± 0.02 (pHm) 10.34 ± 0.01 (UV-vis)
n-octanol/water distribution			
$\log D_{2.0}$ 25 °C $\log D_{7.4}$ 25 °C $\log D_{7.4}$ 37 °C	−2.6 ± 0.01 +2.4 ± 0.1 +2.9 ± 0.1	+0.15 ± 0.01 −1.99 ± 0.06 −1.82 ± 0.05	−0.68 ± 0.02 [a] −0.29 ± 0.02 [a] −0.17 ± 0.03
Species at pH 7.4			
	HL^+: 76% [b] L: 24% [c]	L^-:100%	HL: 100%
Species at pH 2.0			
	H_4L^{4+}: 33% H_3L^{3+}: 62%	HL:100%	H_2L^+: 58% HL: 42%
	H_2L^{2+}: 5%		

[a] Lipophilicity data for the hydrolyzed products h-MOLNU at 25 °C: $\log D_{2.0} = -1.25 \pm 0.04$, $\log D_{7.4} = -2.00 \pm 0.05$; [b] HL^+: 67%, L: 33% using pK_{a4} = 7.7 determined by Szakács et al. [48].

2.3. Lipophilicity

Lipophilicity of the studied drugs has been scarcely reported in the literature [15]. Table 1 comprises the logarithm of distribution coefficients ($\log D_{pH}$) determined at pH 2.0 and 7.4. Imatinib appears to be highly hydrophilic, more than MOLNU, at pH 2.0; however, gradual loss of positive charges provides a rather lipophilic molecule at pH 7.4. Molnupiravir retains its hydrophilic character even at this pH thanks to the polar sugar moiety. Hydrolyzed MOLNU (h-MOLNU, prepared by alkaline hydrolysis of MOLNU) was also studied and it is somewhat more hydrophilic than the parent molecule. Favipiravir was proven to be amphiphilic at pH 2.0 and it is mainly hydrophilic at pH 7.4 where the deprotonated form is

predominant. The *n*-octanol/water distribution of the compounds at pH 7.4 was assayed at 37 °C as well, the coefficients move slightly to the (more) lipophilic range at this temperature.

2.4. Fluorescence Properties of FAVI and IMA

Among the three studied antiviral agents, only FAVI exerts measurable fluorescence emission in aqueous solution as it was shown in the former section (Figure 4). This phenomenon was further investigated in various solvents and fluorescence lifetime parameters were also determined by time correlated single photon counting (TCSPC) (Table 2, Figures S7 and S8). Favipiravir displays the most intense fluorescence when it is deprotonated. A single excitation peak is observed, which corresponds well to the absorption maximum (λ = 362 nm). The neutral form dissolved in water, ethanol or *n*-octanol shows much smaller fluorescence intensity, and the two bands in the excitation spectra reflect the shape of the absorption spectra recorded in the same solvents. As it is known that planar aromatic structures are the most fluorescent, the aromatic character of the deprotonated form can be assumed. In the case of the neutral form, the retained but much lower fluorescence and the dual absorption and excitation bands refer to the parallel existence of more tautomers under this condition, from which one form preserves the aromatic structure. Fluorescence lifetime data confirm the presence of two kinds of fluorophores in acidic aqueous, ethanolic and *n*-octanolic solutions of FAVI. The minor species possess shorter lifetime (τ_1 = 3.8–6.4 ns), while the lifetimes of the longer-lived forms (τ_2 = 8.05–9.74 ns) are rather similar to that of the deprotonated form (τ = 10.00 ns). Our findings suggest that FAVI (or its fluorescent metabolites) is most likely responsible for the fluorescence of nails, hair, skin, face, and sclera of FAVI-treated patients [23–25].

Table 2. Fluorescence parameters of FAVI determined in various solvents: λ(max) of the excitation and emission spectra, relative fluorescence intensities, lifetimes (τ) and relative amplitudes (α) of the lifetime components determined by TCSPC [a] [t = 25 °C].

	λ_{EX} (max) (nm)	λ_{EM} (max) (nm)	Relative Intensity [b]	τ_1 (ns)	τ_2 (ns)	α_1 %	α_2 %
water pH 7.4	362	428	1.00	10.00 ± 0.01	-	100	-
water pH 2.0	322, 365	438	0.16	5.64 ± 0.01	-	100	-
n-octanol	372	435	0.36	6.4 ± 0.2	9.74 ± 0.03	37	63
ethanol	330, 368	432	0.14	3.8 ± 0.1	8.05 ± 0.01	25	75

[a] Determined at λ_{EX} = 360 nm, λ_{EM} = 430 nm; [b] Calculated at λ_{EX} = 370 nm, λ_{EM} = 430 nm.

In both ethanol and *n*-octanol, IMA and MOLNU (and h-MOLNU) fluorescence was minimal in aqueous solution at any protonation state. In *n*-hexane, IMA has weak fluorescence (λ_{EX} = 287nm, λ_{EM} = 450 nm, Figure S9), whereas MOLNU is not in this solvent.

2.5. Interaction with Blood Serum Proteins Human Serum Albumin and α1-Acid Glycoprotein

Our experiments on global serum protein binding and interaction with HSA and AGP are reported in detail in this section, and the acquired results are discussed and compared with literature data in Section 2.6. The diverse aqueous solubility of the compounds required a complex methodological approach to study their serum protein binding. Consequently, this involved the combined use of spectrofluorometry, ^{1}H NMR spectroscopy, ultrafiltration–UV-vis and capillary electrophoresis frontal analysis techniques.

In the first step, the interaction of the three medicines (at 50 μM concentration) with whole human serum was investigated using ultrafiltration. Following the filtration, the low molecular mass (LMM) fraction of the samples was studied by UV-vis spectrophotometry. As depicted in Figure 6, the compounds exhibit diverse behavior. By filtering the compounds dissolved in PBS (dashed spectra), IMA stuck to the filter to a high extent (85%) most likely due to its limited solubility at pH 7.40. Molnupiravir and FAVI could be recovered in 78% and 100% after filtration, respectively. Then compounds were ultrafiltered in the presence of 4-fold diluted blood serum and the adhesion was considered. Practically

no free IMA was detected in solution, FAVI is bound in 18 ± 2% and MOLNU showed no measurable binding to the serum protein fraction. However, the hydrolytic state of MOLNU is not known in this experiment as the hydrolyzed forms (EIDD-1931 and isobutyrate) have the same absorption spectrum as the parent compound. Therefore, the stability of MOLNU was investigated in the presence of blood serum by ^{1}H NMR spectroscopy. MOLNU at 1 mM final concentration was mixed with 2-fold diluted blood serum and the reaction was followed in time as it is shown in Figure 7. The colored frames show well that a new set of peaks appears in the spectra that can be attributed to isobutyrate and EIDD-1931. The hydrolysis is relatively slow and was completed in more than one day (Figure S10). The pseudo-esterase activity of HSA is known from the literature [37,49,50]; furthermore, divalent metal ions such as Cu(II) ion may induce ester hydrolysis as well [51]. Therefore, as a next step, the effect of HSA (630 µM) and the LMM fraction of blood serum, possibly containing traces of Cu(II) ion, was investigated in separate experiments. Neither of the two media could induce hydrolysis of MOLNU within two days. The same behavior was observed in the presence of 15 µM AGP or 45 µM human transferrin. Knowing that orally taken MOLNU does not practically reach the circulatory system, but h-MOLNU does, the serum protein binding studies were done with the hydrolyzed form, which are supplemented with the results obtained for MOLNU for comparison.

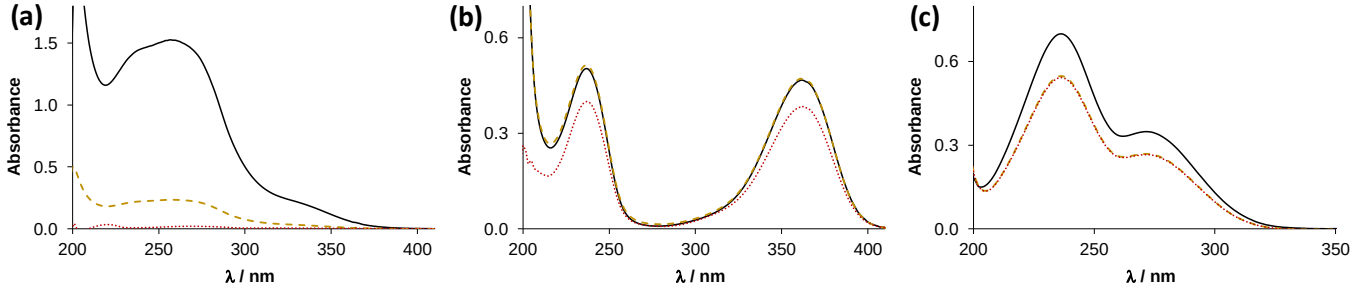

Figure 6. Absorption spectra of ultrafiltered (**a**) IMA, (**b**) FAVI and (**c**) MOLNU in the absence (dashed brown spectra) and in the presence of blood serum (red dotted spectra) plotted together with the non-filtered reference spectra (solid black line) [$c_{compound}$ = 50 µM; 4-fold diluted blood serum; pH = 7.4 (PBS); t = 25 °C]. The red dotted spectra are corrected by the absorption originating from the ultrafiltered blood serum.

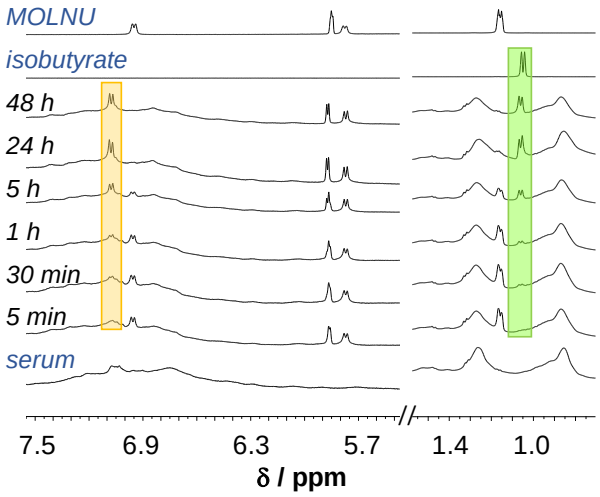

Figure 7. ^{1}H NMR spectra of MOLNU—blood serum system followed in time, colored frames denote the peaks of the hydrolyzed products EIDD-1931 (yellow) and isobutyrate (green); spectra of blood serum, MOLNU and isobutyrate are shown as well [c_{MOLNU} = 1 mM; blood serum: 2-fold diluted; $c_{isobutyrate}$ = 1 mM; pH = 7.4 (PBS), 10% (v/v) D_2O/H_2O; t = 25 °C].

The serum protein binding of h-MOLNU (30 μM) was investigated in ultrafiltration experiments and no binding to HMM components of blood serum or binding to the single proteins HSA (630 μM) or AGP (15 and 30 μM) was observed (Table S1). Interestingly, MOLNU was bound to AGP in 4 ± 1% and 8 ± 1% in the presence of 0.5 and 1 equiv. AGP, respectively, while ultrafiltered samples of blood serum indicated less than 2% binding to the HMM fraction (Table S1). Moreover, for FAVI, less than 2% of the bound fraction of the compound could be detected in ultrafiltration experiments by the addition of different concentrations of HSA or AGP (see Table S1). At the same time, moderate binding to HMM components (ranging from 18 to 28%) was detected when FAVI was dissolved in (diluted or non-diluted) whole blood serum. The highest (28%) serum protein binding of FAVI was found under the conditions being most similar to the physiological ones (200 μM FAVI in non-diluted blood serum). When 50 μM IMA and equimolar HSA was ultrafiltrated, about 40% remained in the HMM fraction (Table S1), however these data should be handled cautiously, due to the high adhesion tendency of the compound to the filter surface.

Due to the adhesion phenomenon of IMA to the ultrafiltration membrane, frontal analysis capillary electrophoresis (FACE) was utilized to investigate the interaction of the drug with HSA and AGP. The FACE technique enables the study of rapid equilibrium processes unlike capillary zone electrophoresis. Herein, a large volume of pre-equilibrated sample was introduced into the capillary, and overlapping plateaus appear in the electroferogram instead of well separated zonal peaks. The concentration of the unbound drug can be determined from the plateau height of the free portion of the drug. The electrophoretic conditions were optimized for first, namely using PBS buffer as BGE and injection time of 30 s resulted in a reasonable plateau shapes and analysis time (Figure 8 and Figure S11). Imatinib is partly positively charged under this condition (Table 1), therefore it migrates before the negatively charged high molecular weight protein. In Figure 8, the effect of increasing amounts of AGP on the plateau height of free IMA can be followed. Gradually decreasing plateau heights are proportional to the free fraction of IMA and formation curve in Figure 8b for the AGP–IMA system can be calculated as well. The curve becomes saturated at an $[IMA]_{bound}/c_{AGP}$ ratio of close to 1, thus binding of maximum one IMA per AGP is feasible. The binding constant $\log K' = 5.2 \pm 0.1$ was calculated with the PSEQUAD program [52] and the fitted binding curve is in good agreement with the experimental data points (Figure 8b). The addition of HSA instead of AGP affected barely the plateau height of IMA, and no considerable binding was found in the presence of up to 5 equiv. albumin. Rather similar behavior was seen in the case of HSA–FAVI and AGP–FAVI chemical systems in FACE studies (see Figure S12 for representative electropherograms recorded for the HSA–FAVI system). This finding is consistent with the observations of ultrafiltration experiments (Table S1).

The protein binding of the title compounds was further investigated by spectrofluorometric measurements. Albumin possesses three main hydrophobic drug binding pockets, referred to as Sudlow's site I (in subdomain IIA), Sudlow's site II (in IIIA) and site III (in IB). In these pockets, HSA binds and transports mostly lipophilic, neutral or negatively charged endogenous and exogenous compounds [37,53]. Binding at site I can be followed by fluorometry directly through the quenching of tryptophan-214 (Trp-214) residue. Moreover, fluorescent site markers such as warfarin (WF, for site I) and dansylglycine (DG, for site II) can be used for site specific binding assays [54,55]. In AGP, there are seven binding sites with varying affinities and capacities, however, all basic drugs, together with the acidic ones, can bind into the hydrophobic central cavity of AGP. For practical purposes, only this binding site may be considered for clinical relevance [36]. The Trp25 and Trp122 residues lie inside and next to the central binding cavity, respectively [40], therefore fluorescence quenching experiments are suitable to follow drug binding here. The displacement of dipyridamole (DIP) from AGP is another, less well-known approach to monitor the binding of a compound to AGP via fluorescence anisotropy measurements [56].

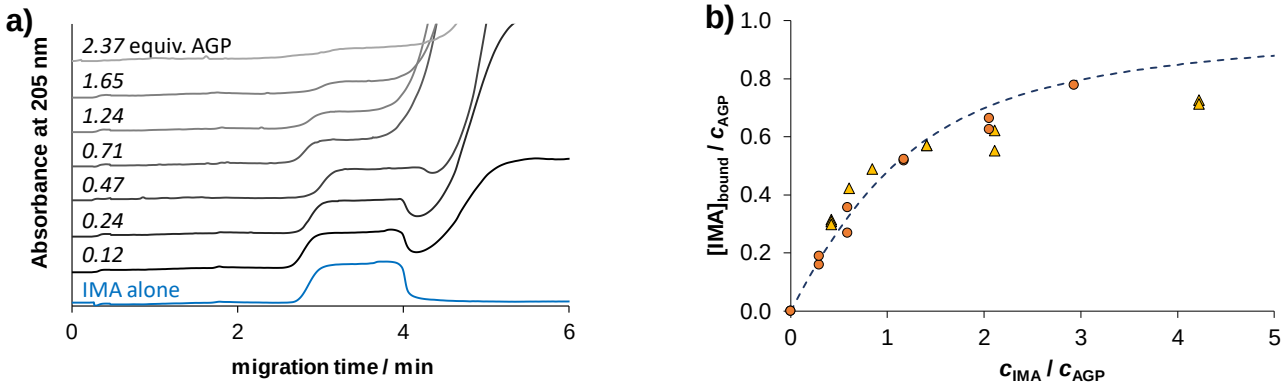

(**a**) (**b**)

Figure 8. (**a**) Electropherograms recorded for the AGP–IMA system where the IMA concentration was constant and protein concentration varied. (**b**) Binding curve derived from the free IMA plateau heights of the same titration (●) and the AGP–IMA titration (▲) together with the binding curve computed on the basis of the determined binding constant (logK' = 5.2 ± 0.1) [c_{IMA} = 15 µM (●) 0–17 µM (▲); c_{AGP} = 0–36 µM (●) 5.6 µM (▲); BGE: pH = 7.4 (PBS); voltage:10 kV, current: 180 µA; t = 25 °C].

The three-dimensional fluorescence spectra in Figure 9 recorded for the AGP–IMA and HSA–IMA systems show well the differences between the binding affinities of the drug to the two proteins. The fluorescence of AGP (at λ_{EX}: 280 nm, λ_{EM}: 325 nm) reduced to ca. 60% upon addition of IMA and in turn the weak induced fluorescence of IMA (at λ_{EX}: 280 nm, λ_{EM}: 465 nm) appears in the spectrum. At the same time, light emission of HSA is barely affected by IMA and the induced fluorescence of the latter could not be observed. Favipiravir did not quench the fluorescence of HSA or AGP under the same conditions, and the presence of the proteins had no effect on the intense fluorescence band of FAVI (see Figure S13 for 3D spectra).

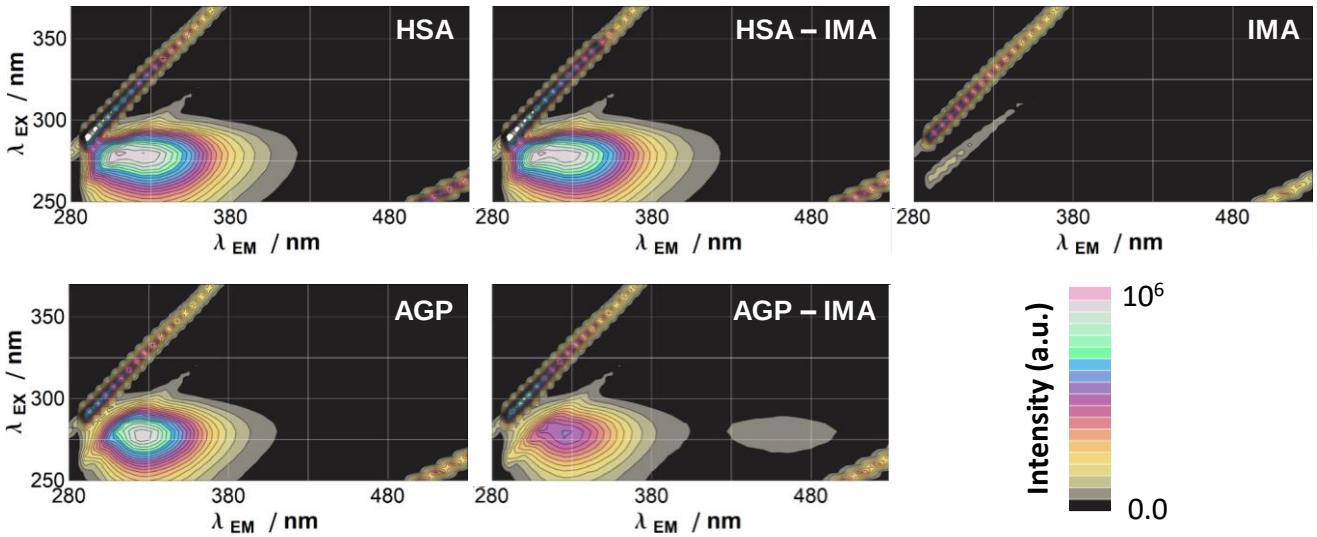

Figure 9. Three-dimensional fluorescence spectra of the HSA–IMA and AGP–IMA systems [c_{HSA} = 1.0 µM; c_{AGP} = 0.53 µM; c_{IMA} = 4.6 µM; pH = 7.4 (PBS); t = 25 °C].

Further titration experiments were carried out, to gain a deeper understanding of the binding interaction. Representative emission spectra obtained from the titration of the AGP–IMA system are presented in Figure 10. The fluorescence of AGP mainly originates from the three Trp amino acid residues. The binding of IMA effectively quenches this fluorescence and, in parallel, the induced emission band of IMA shapes a saturation curve (Figure 10). The position of the emission peak (λ_{EM} = 465 nm) together with the excitation maximum

(λ_{EX} = 280 nm) of the bound IMA resemble to those obtained in *n*-hexane, verifying that the binding takes place in the hydrophobic cavity of the protein. The quenching studies were repeated at 37 °C, and the effect of long-term storage of frozen AGP stock solutions in plastic microtubes was investigated as well. The reason for the later experiment was, that plasticizers used for plastic containers and rubber wares can reportedly disrupt the binding of drugs to AGP [36,57]. All spectra were used for computing quenching constants shown in Table 3 with the computer program PSEQUAD [52], and a very good match was found between the experimental and calculated fluorescence intensities (see an example in Figure 10b). The determined values indicate that the binding affinity is somewhat higher at 37 °C in contrast to the constant obtained at room temperature (logK' = 6.0 ± 0.1 vs. 5.8 ± 0.1, respectively). The effect of the long-term storage in plastic microtubes on the binding ability of AGP also appears to be moderate (ΔlogK' = 0.2).

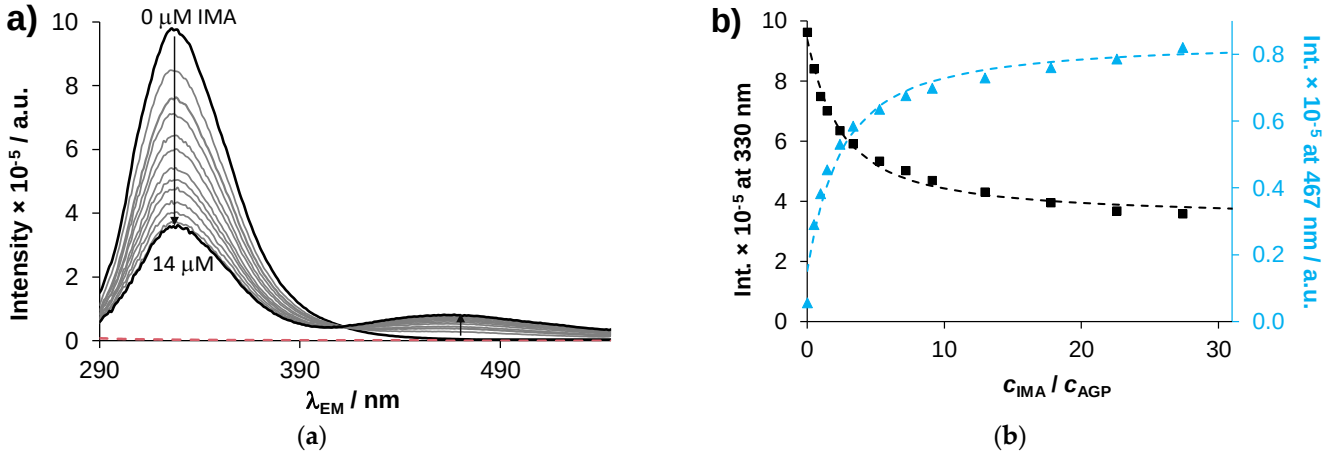

Figure 10. (**a**) Quenching of AGP fluorescence by addition of IMA and emission spectrum of IMA alone (red dashed line, 50 μM). (**b**) The measured and computed (dashed lines) emission intensities (Int.) at 330 nm (■) and 448 nm (▲) [c_{AGP} = 0.53 μM; c_{IMA} = 0–47 μM; λ_{EX} = 280 nm; pH = 7.4 (PBS); t = 25 °C].

Figure 11 shows little quenching when AGP was titrated with FAVI, h-MOLNU, or MOLNU. Even 91 equiv. of FAVI quenched in only 6% the fluorescence of AGP (Figure S14), and the emission band of FAVI itself (see Figure S14 at 430 nm) is barely affected in the presence of this protein. Both h-MOLNU and MOLNU, similarly to FAVI, did not quench the fluorescence of AGP.

The binding of IMA, h-MOLNU and FAVI to AGP was also investigated in dipyridamole (DIP) displacement experiments. Dipyridamole is a drug utilized for decreasing platelet aggregation and for coronary vasodilatation. It binds to AGP at one site with extremely high affinity that is located in the hydrophobic pocket of the glycoprotein, and at least one additional low affinity site for DIP is assumed as well [58]. Dipyridamole is highly fluorescent in the visible range ($\lambda_{max(EX)}$ = 400 nm, $\lambda_{max(EM)}$ = 500 nm) and its steady-state fluorescence spectrum was not very sensitive to the binding on AGP (Figure S15). On the other hand, fluorescence anisotropy is an excellent method to follow the protein binding of DIP. Briefly, fluorescence anisotropy experiments provide information on the size and shape of a fluorophore via measurement of the polarized emission of a solution [59]. AGP-bound DIP possesses much higher anisotropy due to the slower rotational diffusion of the protein in comparison to free DIP (own data: $r_{bound} \approx 0.25$; $r_{free} \approx 0.003$; at pH = 7.40 (PBS), 25 °C). As Figure 12 shows, a considerable amount of DIP is bound to AGP (r = 0.14) under the applied conditions, and the anisotropy of the sample decreases by the addition of IMA in line with the increase of free and rapidly rotating fraction of DIP. It is noteworthy that h-MOLNU was not able to displace DIP from its binding pocket (Figure 12). The same experiment performed with FAVI is a good example to draw attention to the possible false interpretation of fluorescence anisotropy data where the hypothesized competitor

itself (FAVI) displays fluorescence under the conditions used. A decrease in anisotropy is also observed here, however (according to the ultrafiltration, FACE, and fluorescence quenching experiments) no interaction between the studied species takes place (see details under Figure S16). Taking advantage of the intrinsic fluorescence of FAVI, direct measurements on its fluorescence anisotropy were carried out in the absence and presence of AGP. The anisotropy value did not increase considerably in the presence of 10 equiv. AGP ($r_{\text{free FAVI}} = 1.8 \times 10^{-3} \pm 4 \times 10^{-4}$, $r_{\text{FAVI with AGP}} = 2.5 \times 10^{-3} \pm 5 \times 10^{-4}$).

Table 3. Binding constants (K') reported in the literature and determined [a] in this study for the AGP–IMA and HSA–IMA systems under the indicated conditions.

Protein (Variant/Type) {Storage}	pH (Buffer)	T/°C	Method	K'	logK'	Reference
AGP	4.95 (acetate)	25	ITC [b]	8.7×10^2	2.94	[27]
	4.95 (acetate)	25	NMR [c]	3.2×10^3	3.51	
	(PBS)	n.d. [d]	ultrafiltration	4.9×10^6	6.69	[32]
(native)	7.4 (ringer)	37	circular	2.4×10^6	6.38	[26]
(F1-S)	7.4 (ringer)	37	dichroism	1.7×10^6	6.23	
{glass, freshly prep.}	7.4 (PBS)	25	fluorometry	6.3×10^5	5.8 ± 0.1	present study
{plastic, 2 months} [e]	7.4 (PBS)	25	fluorometry	1.0×10^6	6.0 ± 0.1	
{glass, freshly prep.}	7.4 (PBS)	37	fluorometry	1.0×10^6	6.0 ± 0.1	
{glass, freshly prep.}	7.4 (PBS)	25	FACE	1.6×10^5	5.2 ± 0.1	
HSA	(PBS)	n.d.d	ultrafiltration	2.3×10^5	5.36	[32]
(fatty acid free)	7.0 (phos.) [f]	20	fluorometry	1.2×10^5	5.08 [g]	[28]
(fatty acid free)		37	fluorometry	1.0×10^5	5.02 [g]	
	7.4 (phos.) [f]	27	fluorometry	1.3×10^5	5.1	[31]
	7.4 (phos.) [f]	37	fluorometry	1.0×10^5	5.0	
	7.4 (ringer)	rt [h]	affinity LC [i]	~3×10^4	4.5	[26]
	7.4 (PBS)	25	fluorometry	$\leq 10^4$	≤ 4.0	present study
	7.4 (PBS)	37	fluorometry	$\leq 10^4$	≤ 4.0	
	7.4 (PBS)	25	FACE	no binding found		

[a] Determined from at least two parallel measurements; [b] ITC: isothermal titration calorimetry; [c] NMR: spin-lattice relaxation times; [d] n.d.: non-defined; [e] Stored in microcentrifuge tube at −20 °C for 2 months; [f] phos.: phosphate; [g] Reported originally as dissociation constants: $K_d = 8.3 \times 10^6$ (logK' = 5.08), $K_d = 9.6 \times 10^6$ (logK' = 5.02) [28]; [h] rt: room temperature; [i] LC: liquid chromatography.

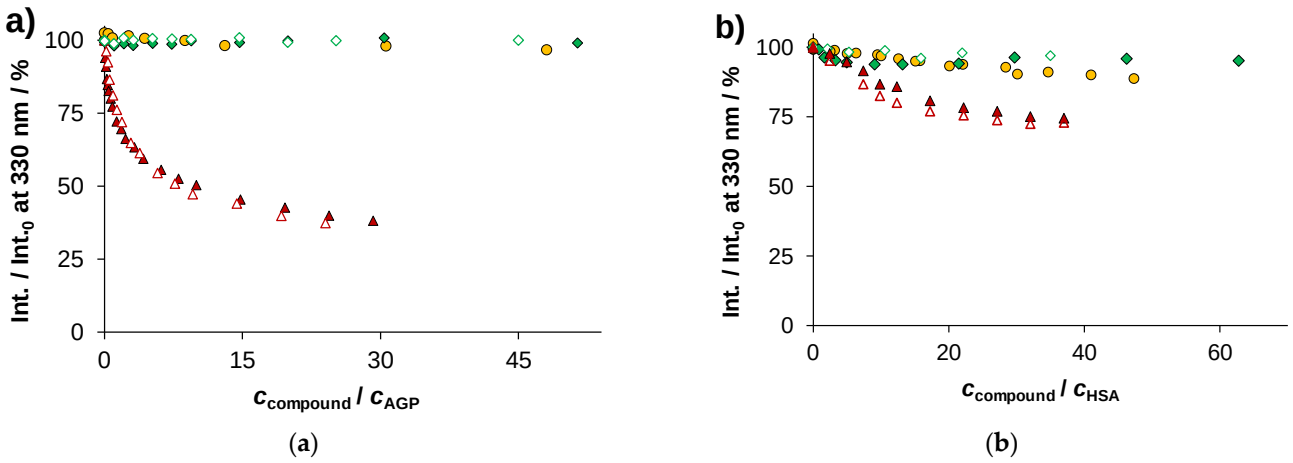

Figure 11. Comparison of the quenching effect of IMA (▲), FAVI (●), h-MOLNU (◊) and MOLNU (♦) on the fluorescence of (**a**) AGP or (**b**) HSA at 25 °C; the quenching experiments with IMA were measured at 37 °C as well (Δ) [c_{AGP} = 0.5 μM; c_{HSA} = 1 μM; λ_{EX} = 280 nm; λ_{EM} = 330 nm; pH = 7.4 (PBS)].

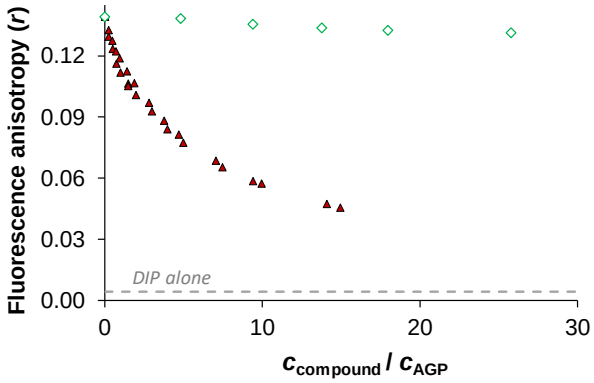

Figure 12. Fluorescence anisotropy (r) of the AGP–DIP system in the absence and presence of IMA (▲) or h-MOLNU (◊); anisotropy signal of free DIP (grey dashed line, $r = 3.0 \times 10^{-3} \pm 8 \times 10^{-4}$) is indicated as well [$c_{AGP}$ = 2.0 μM; c_{DIP} = 1.0 μM; λ_{EX} = 400 nm; λ_{EM} = 500 nm; pH = 7.4 (PBS), t = 25 °C].

Binding events at the hydrophobic sites of HSA were investigated in Trp-214 quenching and site marker displacement experiments. Both WF and DG are high affinity fluorescent markers of hydrophobic sites I and II, respectively. The Trp-214 quenching also provides information on the binding at site I. The Trp-214 fluorescence was weakly quenched by the addition of IMA to HSA, and only 25% and 27% quenching was observed by the addition of 37 equiv. Imatinib at 25 °C and 37 °C, respectively (Figure 11b). Based on these data, the binding constants $\log K' \leq 4.0$ were estimated. The WF displacement experiments displayed no replacement of bound WF, on the contrary a small, 17% increase of the fluorescence can be observed (Figure S17). This cannot be explained by the induced fluorescence of IMA, as it did not show any fluorescence by the addition of HSA (in contrast to AGP) (see Figure 9). Possibly the weak binding of IMA elsewhere results in somewhat different arrangement of interacting moieties in site I, e.g., more hydrophobic environment around bound WF. Imatinib was unable to displace DG from the hydrophobic site II of HSA (Figure S18). Thus, no binding constants could be calculated from the site marker displacement experiments. Similarly, FAVI, h-MOLNU and MOLNU did not significantly quench the fluorescence of Trp-214 (Figure 11 and Figure S19). The WF displacement studies also showed no competition of these compounds for site I. No measurement was applicable for the HSA–DG–FAVI ternary system due to the overlap of fluorescence bands of DG and FAVI. Based on our data, h-MOLNU and MOLNU could not displace DG from site II.

2.6. Discussion of the In Vitro Blood Serum Distribution of the Compounds

Studying the in vitro hydrolysis of MOLNU in blood serum appears to be a theoretical problem, because orally administered MOLNU is hydrolyzed by carboxylesterases during or after absorption to deliver EIDD-1931 into the systemic circulation [15]. At the same time, it may be important to monitor the fate of MOLNU following intravenous administration, where the drug directly enters the circulation. Our results showed relatively slow (ca. one day) hydrolysis of MOLNU in whole blood serum, which is clearly due to the presence of HMM components. The rate of the hydrolysis can be somewhat different at physiological conditions, where, in contrast to the experimental conditions 37 °C and low micromolar concentration of MOLNU applies. Human serum albumin is an obvious suspect, as its pseudo-esterase activity was demonstrated in numerous experiments with respect to acetylsalicylic acid, fatty acid esters, ketoprofen glucuronide, cyclophosphamide etc. [37,49,50]. Nevertheless, HSA could not hydrolyze the ester bond of MOLNU. Besides HSA, butyrylcholinesterase (pseudo-cholinesterase), and paraoxonase exerts esterase activity in blood plasma and traces of acetylcholinesterase (8 ng/mL) are present as well in blood [50]. The typical substrates of paraoxonase are likely phosphate esters, therefore butyrylcholinesterase, present in ca. 2.3–6.8 μg/mL in blood plasma, is more likely responsible for the enzymatic cleavage of the ester bond in MOLNU [50,60]. In fact, hydrolysis of MOLNU is likely to be faster in circulating blood due to the extensive esterase activity of the liver [61]. The present studies implemented

by ultrafiltration and spectrofluorometric techniques indicated no considerable binding of h-MOLNU or MOLNU to serum proteins.

To the best of our knowledge, the binding of FAVI to human serum proteins was only investigated in vitro. The Japanese product monograph of Avigan® tablets reports a 53–54% protein bound fraction of FAVI (c_{FAVI} = 1.7–173 μM); furthermore, the binding was attributed to HSA and AGP in 65% and 6.5%, respectively [14]. There is confusion in the literature, as the 54% overall protein binding of FAVI is commonly cited as in vivo data [17–21], although the adverted sources (if they are indicated) also seem to use this value as a non-referred literature data [20]. Moreover, this value is practically identical with the producer's in vitro data (vide supra). Unfortunately, the monograph is not very detailed on the methodology: ultrafiltration was done, most probably by mixing of blood serum samples of various species (dog, rat, rabbit, human; obtained in advance) with FAVI; and it is not clear what kind of additional analytical method was applied to determine the bound HSA-to-AGP ratio [14]. The in vivo serum protein binding assays were performed only on rats and monkeys [14]. In vitro ultrafiltration experiments in the present study showed ca. 28% binding of FAVI to the HMM fraction of whole blood serum when 200 μM drug (corresponding to an average blood plasma level [14]) was interacted with non-diluted human blood serum. In addition, our ultrafiltration (Table S1) and FACE studies implemented with single proteins HSA and AGP strongly suggest that neither of the two proteins are involved in binding of FAVI. Our spectrofluorometric assays also confirmed these observations. Discrepancies between the literature and present data may originate from the different methodology applied, or possible ethnic or regional differences should be taken into account in future studies, as it was noted in regards of the differing plasma levels of FAVI in Japanese patients and patients form the US [21].

Clinical relevance of serum protein binding of IMA is widely reported [29,33,38,57]. The role of AGP has been demonstrated in several in vivo and in vitro studies [32,33,38,39]. Elevated blood level of AGP was associated with delayed or lack of response to IMA treatment [33,57]. On the other hand, some studies reported low affinity or no binding of IMA to AGP [27,62]. These latter observations are possibly due to the non-physiological conditions applied (Table 3) [27] or to the pre-treatment of AGP used for the assays [62]. Moreover, it has long been reported that plasticizers can disrupt the binding of drugs to AGP; the impact of diethylhexyl phthalate (DEHP), released from PVC blood collection bags, on the free fraction of IMA in human plasma was also assessed [63]. Although microcentrifuge tubes are generally made of polypropylene, several water soluble leachables are found in them as typical processing agents and additives, including aromatic agents (e.g., 3,4-dimethylbenzaldehyde, Millad-3988) [64]. Our results showed only a little deviation between the computed binding constants when AGP stock solution was prepared freshly or stored for 2 months in 'low-price' plastic microtube at −20 °C ($\log K' = 5.8 \pm 0.1$, 6.0 ± 0.1, respectively). The binding affinity was also somewhat higher when samples were thermostated at 37 °C ($\log K' = 6.0 \pm 0.1$) instead of 25 °C; however, the difference, just like in the previous relationship, was not significant. These constants are somewhat lower than those reported by Fitos et al. and Gambacorti-Passerini et al., but fall within the same range and reveal high affinity binding of IMA on AGP [26,32]. The FACE experiments yielded an overall AGP–IMA binding constant ($\log K' = 5.2 \pm 0.1$) that was approximately four times lower than the spectrofluorometric quenching data. Similarly, no binding could be observed when the interaction of IMA with HSA was monitored by FACE, however, fluorometric quenching and ultrafiltration studies demonstrated weak binding here. It seems, that electrophoretic conditions favor dissociation of IMA-protein adducts, however this observation would require more detailed investigations. Albumin binding of IMA was generally considered less important in clinical practice, however binding constants reported in the range of $K' = 10^4$–10^5 are considerable (Table 3). Among these reports, Di Muzio et al. used fatty acid free HSA and applied rather high IMA concentrations for the fluorometric assays without correction of the intensities by inner filter effect [28]. Gambacorti-Passerini et al. carried out ultrafiltration experiments, however it is not clear how they accounted for adhesion to the filter [32]. This uncertainty also applies for their AGP binding constant [32]. The results of the

present study suggest a stability constant about one order of magnitude lower for the HSA–IMA adduct, which is in relatively good agreement with the data reported by Fitos et al. [26].

To illustrate the effect of the uncertainty in the HSA–IMA binding constant, model calculations depicted in Figure 13 were carried out. Variation of total concentrations of IMA and AGP on the free levels of IMA in blood was modelled as well. Figure 13a shows well, that, albumin has considerable impact on the distribution of IMA only if the HSA–IMA binding constant is $K' > 10^3$ and the concentration of AGP corresponds to the normal average level (15 μM) [36]. An average total peak concentration (c_{max}) of IMA in blood serum is reported to be 2 μM, its free fraction slightly decreases from ca. 7% to 5% if the HSA–IMA constant $K' = 10^4$ (the upper limit of our fluorometric estimation) applies instead of $K' = 10^3$. The relevance of albumin binding further lessens with two- and three-fold elevated AGP levels (Figure 13b,c), and less than 4% of total IMA is unbound under these conditions. In all, the AGP binding of IMA is more important compared to HSA. Moreover, AGP has a relatively low normal plasma level, but in acute-phase response a two- or three-fold increase in its concentration results in reduction of free IMA level to one half or one third in comparison to the one observed under physiological conditions according to the model calculations (Figure 13). This finding explains why elevated AGP levels may prevent the efficacy of IMA [32,38].

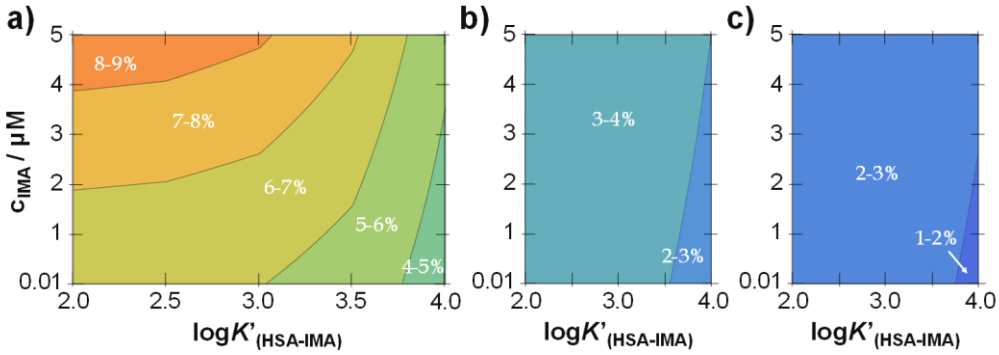

Figure 13. Model calculations on the free fraction (%) of IMA in blood serum by variation of the total concentration of IMA (0.01–5 μM), the HSA-IMA stability constant and the total concentration of (**a**) AGP: 15 μM, (**b**) 30 μM or (**c**) 45 μM [log$K'_{(AGP-IMA)}$ = 6.0].

3. Materials and Methods

3.1. Materials

The antiviral agents FAVI, IMA and MOLNU are products of MedChemExpress (Monmouth Junction, NJ, USA); WF, DG, DIP, D_2O, HSA (A8763, essentially globulin free), AGP (G9885), transferrin (T3309, containing physiological amount of iron) and human blood serum (H4522, male AB plasma) were purchased from Sigma–Aldrich (Merck KGaA, Burlington, MA, USA). Inorganic compounds such as KCl, NaCl, KH_2PO_4 and $Na_2HPO_4 \times 2\ H_2O$, boric acid, sodium trimethylsilylpropanesulfonate (DSS), 2-(*N*-morpholino)ethanesulfonic acid (MES) and 4-(2-hydroxyethyl)-1-piperazineethanesulfonic acid (HEPES) were products of Molar Chemicals (Halásztelek, Hungary) or Reanal (Budapest, Hungary) in puriss quality.

3.2. Stock Solutions and Sample Preparation

For preparation of stock solutions and samples, Milli-Q water was used. Stock solutions of FAVI and MOLNU were prepared in water or in phosphate buffered saline (PBS, pH = 7.40) in 1–10 mM concentration. Imatinib could be dissolved in 0.01 M hydrochloric acid (c = 10 mM). The HSA, AGP and transferrin stock solutions were prepared in PBS buffer (pH = 7.40). The concentration of HSA and AGP stock solutions was determined on the basis of the reported molar absorbances: ε(280 nm) = 36,850 $M^{-1}cm^{-1}$ ε(280 nm) = 24,140 $M^{-1}cm^{-1}$, respectively [65–67]. The concentration of transferrin stock solutions was determined based on the average molar weight reported by the producer and calculated molar absorbance at

280 nm fall between the reported values of the apo- and holoprotein [68]. Stock solutions of WF and DG were prepared as described previously [54]. Hydrolyzed MOLNU (h-MOLNU) solutions composed of EIDD-1931 and isobutyric acid were prepared by incubating MOLNU at alkaline conditions (pH ~ 12) for 2 h. All protein containing samples were prepared in PBS and incubated usually at room temperature or at 37 °C for some of the measurements.

3.3. pH-Potentiometry

pH-potentiometric titrations of the antiviral agents were carried out similarly to our former works [69,70]. Proton dissociation constants (K_a) were determined for the compounds at I = 0.1 M KCl, 25 °C with the Hyperquad2013 software [71–73].

3.4. Thermodynamic Solubility (S)

The thermodynamic solubility of IMA was measured for the saturated solutions in water at various pH values (pH 2: 0.01 M HCl, pH 6: 20 mM MES) buffer), pH 7.4 and 8.2: 20 mM HEPES buffer) at 25.0 ± 0.1 °C. Solutions in 10 mM concentration were attempted to make. Samples were mixed overnight, then sedimentation of the solid fraction was forced by centrifugation (Eppendorf, MiniSpin Plus centrifuge, 15 min, 12 000 rpm). The concentration of the compounds was determined by UV-vis spectrophotometry using stock solutions of the compound with a known concentration dissolved in DMSO, 50% and 10% (v/v) DMSO/buffered aqueous solution for the calibration. In the case of FAVI and MOLNU 10 mM solutions at pH 2 and 7.4 could be prepared without the presence of non-dissolved compound.

3.5. Lipophilicity

Distribution coefficient (D_{pH}) values of the compounds were determined by the traditional shake-flask method in *n*-octanol/buffered aqueous solution at various pH values at 25.0 ± 0.2 °C. The pH values of the samples were adjusted with *n*-octanol pre-saturated aqueous solutions containing different buffer systems in ca. 20 mM concentration and 0.10 M KCl. The buffer systems used were as follows: pH 2: 0.01 M HCl; pH 4–6: MES and its Na-salt; pH 6–8: NaH_2PO_4/Na_2HPO_4; pH 8–10: boric acid/borate. Compounds were dissolved in buffered aqueous solutions pre-saturated with *n*-octanol. The final compound concentration was 10−200 μM, and the pH values were precisely monitored. Stock solutions and water pre-saturated *n*-octanol were gently mixed in 1:1, 1:0.1 or 1:0.01 volume ratio for 2 h. After phase separation, the UV-vis spectrum of the compound in the aqueous phase was compared to that of the original stock solution and the D_{pH} values of the compounds were calculated according to the following equation:

$$D_{pH} = \left[\frac{\text{Abs}_{(stock.\ sol.)}}{\text{Abs}_{(aqueous\ phase\ after\ separation)}} - 1 \right] \times \frac{\text{V}_{(aqueous\ phase)}}{\text{V}_{(n-octanol)}}$$

An Agilent Cary 8454 diode array spectrophotometer (Agilent Technologies, Santa Clara, CA, USA) was used to measure the UV-vis spectra in the interval 200–500 nm. The pH dependency of the D_{pH} values was used to estimate the proton dissociation constants (K_a) of FAVI and IMA, as stated in our previous work [74].

3.6. ^{1}H NMR Spectroscopy

^{1}H NMR spectroscopic measurements were carried out on a Bruker Avance III HD instrument (Billerica, MA, USA). The spectra were recorded with WATERGATE water suppression pulse sequence using DSS internal standard and 10% (v/v) D_2O. Aqueous stability of MOLNU was followed at pH 2.0, 7.4 and 12.0. Interaction between MOLNU (1 mM) and HSA (630 μM), AGP (15 μM), transferrin (45 μM) or 2-fold diluted blood serum was studied in PBS buffer. Quantification of h-MOLNU in Figure S10 was done as follows: the spectra containing MOLNU were subtracted by the spectrum of the serum, then the

peak at ca. δ = 1.2 ppm corresponding to h-MOLNU was integrated, the saturation phase of the plot was aligned to 100%.

3.7. Spectrofluorometry

Steady-state fluorescence studies were implemented by a Fluoromax (Horiba Jobin Yvon, Longjumeau, France) fluorometer in 1 cm quartz cells. All samples contained 1–5 μM HSA or 0.5 μM AGP and various protein-to-antiviral agent ratios (up to ca. 60 μM compound concentrations) were used. Site marker displacement experiments were also carried out. In these setups, the HSA-to-site marker (WF or DG) ratio was 1:1 and the concentration of the antiviral compounds was varied. Instrumental settings are listed in Table S2. The computer program PSEQUAD was used for calculation of binding constants (K') for protein–antiviral compound adducts similar to the approach described in our former works [52,54,75]. Calculations were always based on data obtained from at least two independent measurements. Corrections for self-absorbance and inner filter effect were done as described in our former works using the formula suggested by Lakowicz [54,59,75].

Fluorescence anisotropy measurements were made for the AGP–DIP–drug systems (2 μM–1 μM–0–50 μM IMA, MOLNU or FAVI) and AGP–FAVI (5 μM to 0.5 μM) samples. The fluorescence anisotropy signal ®of DIP or FAVI was followed (see wavelength settings in Table S2) by the use of an automated polarizer set mounted into the steady-state instrument. Emission intensity was measured at *HH*, *HV*, *VV*, and *VH* (*H* = horizontal, *V* = vertical) orientations of the polarizers (placed on the excitation and emission sides, respectively) repeatedly, until the relative standard deviation of *r* decreased below 2% or a maximum of 15 cycles were run. The *G*-factor was determined separately as well, $G = Int._{HV}/Int._{HH} = 0.94$. The FluorEssence (v.3.9) software automatically calculated the overall anisotropy according to the equation $r = (Int._{VV} - Int._{VH} \times G)/(Int._{VV} + 2 \times Int._{VH} \times G)$ [59]. The overall fluorescence anisotropy ($\bar{r}$) of a system is equal to the intensity weighted (f_i) sum of the anisotropies (r_i) of each component: $\bar{r} = \Sigma \{(r_i \times f_i)/\Sigma f_i\}$. Consequently, only those ternary systems can be interpreted simply, where (i) the fluorescence intensity of the marker is barely sensitive to the protein binding ($f_{free} \approx f_{bound}$) and (ii) the competitor together with (iii) the protein are not fluorescent under the applied conditions.

The fluorescence lifetime of FAVI was measured on the same fluorometer equipped with a DeltaHub TCSPC controller using NanoLED light source N-360 (Horiba Jobin Yvon). The resolution of the system was 25 ps. See details on the instrument settings in Table S3. Ludox® (from Sigma–Aldrich) was used as scatter solution to obtain the instrument response function (IRF). The background (obtained with blank samples) was subtracted from the decay. The program DAS6 (version 6.6.; Horiba, Jobin Yvon) was used for the analysis of the experimental fluorescence decays. The fluorescence intensity (*Int.*) decay over time is described by a sum of exponentials,

$$Int.(t) = \sum_{i=1}^{n} \alpha_i exp\left(\frac{-t}{\tau_i}\right) \quad (1)$$

where α_i and τ_i are the normalized amplitude and lifetime of component *i* respectively. The quality of the fit was judged from a χ^2_R value close to 1.0 ($\chi^2_R \leq 1.20$) and a random distribution of weighted residuals.

3.8. UV-Visible Spectrophotometry

An Agilent Carry 8454 diode array spectrophotometer was used to obtain UV-vis spectra in the interval 190–1100 nm, the path length (*l*) was 1 cm. The spectrophotometric titrations were performed with samples containing 25–200 μM compound over the pH range 2.0–11.5 at an ionic strength of 0.10 M (KCl) and at 25 °C. Proton dissociation constants together with the individual molar absorbance spectra were calculated with the computer program PSEQUAD [52]. The program requires the following input data: measured spectra together with the corresponding pH and analytical (total) concentration of the compounds; species matrix, with approximate protonation constant(s) and the absorbing species need

to be defined. The Newton–Raphson iterative method was used to obtain protonation constant(s) with standard deviations and molar spectra of the individual species.

3.9. Ultrafiltration

Samples were separated by ultrafiltration through 10 kDa membrane filters (Millipore, Amicon Ultra-0.5) into low and high molecular mass (LMM and HMM) fractions as described in our former work [54]. Samples contained various amounts of HSA (50–630 μM) or AGP (15–30 μM) and 25–200 μM antiviral agents. Blood serum was used without dilution or diluted to 2- or 4-fold with PBS. The concentration of the non-bound compounds in the LMM fractions was determined by UV-vis spectrophotometry by comparing the recorded spectra to those of reference samples without the protein. The LMM fraction of ultrafiltered blood serum possesses absorbance between 200 and 300 nm, which was taken into account during treatment of the spectra of samples containing the antiviral compounds and serum as well.

3.10. Capillary Electrophoresis

Frontal analysis capillary electrophoresis (FACE) measurements were performed on an Agilent 7100 capillary electrophoresis system Santa Clara, CA, USA) equipped with a diode-array detector (210–600 nm). For all experiments bare fused silica capillaries of 48 cm total length (50 μm inner diameter) were used (BGB Analytik, Boeckten, Switzerland). The background electrolyte (BGE) was PBS buffer (pH 7.40). The conditioning process of new capillaries and daily preparation were done as described formerly [55]. In order to ensure the steady baseline, the capillary was flushed with BGE (2 min) before each run and was rinsed with NaOH (0.1 M; 1.5 min), H_2O (1.5 min), and then with BGE (2 min) after each separation. The sample tray and the capillary were kept at a constant temperature of 25 °C. Samples were injected hydrodynamically at 50 mbar for 30 s, and voltage of 10 kV was applied for the separation process producing a current of ca. 180 μA. Electropherograms were recorded and evaluated by the program ChemStation (Agilent Technologies). Protein-to-compound concentration ratio was between 0:1 and 5:1, the compound concentration was usually kept constant (c_{IMA} = 15 μM, c_{FAVI} = 30 μM), and concentration of HSA or AGP was varied. Samples containing IMA in various concentration (0–16 μM) and constant AGP concentrations (5.6 μM) were made as well. The concentration of the non-bound compound was calculated from plateau heights using external calibration.

3.11. Model Calculations

Model calculations were done with the software MEDUSA (32 bit version) [76] using $\log K'_{HSA\text{-}IMA}$ = 2.0–4.0; $\log K'_{AGP\text{–}IMA}$ = 6.0; c_{IMA} = 0.01–5 μM; c_{HSA} = 630 μM, and c_{AGP} = 15, 30 or 45 μM.

4. Conclusions

Serum protein binding of three approved antiviral drugs, FAVI, MOLNU and IMA, used to treat COVID-19 was investigated in this work. In addition to the protein binding assays, proton dissociation processes, aqueous solubility, stability, and lipophilicity at various pH values were also studied by means of pH-potentiometry, UV–visible and fluorescence spectroscopies, and/or by *n*-octanol/water partition experiments. The lipophilicity of the three drugs differs significantly and is highly dependent on the milieu, either they are in the gastric juice (a typical acidic pH: 2.0) or circulating in the blood at pH 7.4. A clear correlation is visible for IMA regarding its actual protonation state and lipophilicity. At pH 2.0, IMA is extremely hydrophilic ($\log D_{2.0} = -2.6$) and exceedingly soluble in water (S > 10 mM), with the majority of the pH 2.0 present in the solution as +3 and +4 charged cations. At pH 7.4, the basic groups of IMA are primarily deprotonated, with a 3:1 ratio of the +1 charged form to the neutral species. Therefore, IMA is rather lipophilic at this pH ($\log D_{7.4}$ = +2.4) and possesses poor aqueous solubility (S = 24 μM, 37 °C). Molnupiravir and h-MOLNU are hydrophilic at both acidic and neutral pH due to the sugar moiety; it

is charge neutral at the pH of the blood, while about half of it is already +1 charged at pH 2.0. A second proton dissociates at pH > 9, and the ester bond in MOLNU hydrolyzes at pH 12.0 rapidly resulting in the formation of EIDD-1931 and the isobutyrate ion. In contrast to the former two agents, FAVI is slightly lipophilic at pH 2.0 ($\log D_{2.0}$ = +0.15) and becomes very hydrophilic when it gets deprotonated and −1 charged above pH 4 ($\log D_{7.4}$ = −1.99). Both FAVI and MOLNU are well soluble in water between pH 2.0 and 8.2. The actual protonation states of the compounds provide a satisfactory explanation for the observed lipohilic-hydrophilic tendencies. Favipiravir is highly fluorescent in its deprotonated form in aqueous solution, but shows less fluorescence in ethanol, *n*-octanol, and water, at pH < 4. Fluorescence lifetime data were also determined in these media.

The distribution of the compounds in blood was investigated in whole serum and in binding experiments with selected transport proteins HSA and AGP by means of membrane ultrafiltration, frontal analysis capillary electrophoresis, steady-state fluorometry, and fluorescence anisotropy techniques. The ester bond in MOLNU is hydrolyzed rather slowly by the protein constituents of blood serum (takes about one day and the hydrolysis is most likely catalyzed by butyrylcholinesterase. This may be important if MOLNU was delivered intravenously into the vascular system. Molnupiravir and its hydrolyzed form do not bind considerably to the HMM fraction of blood serum. Favipiravir bound 18–28% to the protein fraction of blood serum in membrane ultrafiltration experiments but did not show any binding to HSA or AGP in ultrafiltration, capillary electrophoresis and fluorometric studies. This observation contradicts the only available literature data indicating 54% protein binding in vitro, where albumin was indicated as major carrier. To resolve this contradiction in the future, we recommend taking into account any ethnic disparities, in addition to rigorous analysis design. Imatinib strongly binds to AGP, the binding constant varies within $\log K'$ = 5.8–6.0 depending slightly on the temperature (25 °C or 37 °C) or the storage mode of the protein. Fluorometric experiments revealed a much lower affinity for albumin ($\log K' \leq 4.0$ at 25 °C and 37 °C). The FACE experiments indicated weaker binding of IMA towards AGP and no binding to HSA at 25 °C. This underestimation may result from the electrophoretic conditions (electric current, high voltage) or from the frontal analysis technique. We could model the blood distribution of IMA under physiological and pathological conditions using the binding data determined in this study. Model calculations for the IMA–AGP–HSA ternary system revealed that AGP levels play a more important role in the free fractions of IMA than HSA. Our model explains well the clinical observations that elevated AGP levels seemed to prevent the anticancer effect of IMA.

With the present work, we also aimed to point out that it is worthwhile to perform in vitro solution chemistry and biodistribution studies on approved drugs to interpret the phenomena already observed in vivo on patients (e.g., fluorescence of FAVI, possible inefficacy of IMA in the acute phase) and to complement the literature with this context.

Supplementary Materials: The supporting information can be downloaded at: https://www.mdpi.com/article/10.3390/ijms24032849/s1.

Author Contributions: Conceptualization, É.A.E. and O.D.; data curation, O.D., funding acquisition, É.A.E. and O.D.; investigation, O.D.; visualization, O.D.; writing—original draft, O.D.; writing—review and editing, O.D. and É.A.E. All authors have read and agreed to the published version of the manuscript.

Funding: This work was supported by the National Research, Development and Innovation Office-NKFIA (Hungary) through projects PD 131472 and TKP-2021-EGA-32. O.D. gratefully acknowledges the financial support from a J. Bolyai Research Fellowship (bo-125-20). The support of the 'Lendület' Programme (ELKH, LP2019–6/2019) is also acknowledged.

Institutional Review Board Statement: Not applicable.

Informed Consent Statement: Not applicable.

Data Availability Statement: Authors can confirm that all relevant data are included in the article.

Conflicts of Interest: The authors declare no conflict of interest.

References

1. Bernal, A.J.; Gomes da Silva, M.M.; Musungaie, D.B.; Kovalchuk, E.; Gonzalez, A.; Delos Reyes, V.; Martín-Quirós, A.; Caraco, Y.; Williams-Diaz, A.; Brown, M.L.; et al. Molnupiravir for Oral Treatment of COVID-19 in Nonhospitalized Patients. *N. Engl. J. Med.* **2021**, *386*, 509–520. [CrossRef]
2. Ghasemnejad-Berenji, M.; Pashapour, S. Favipiravir and COVID-19: A Simplifed Summary. *Drug Res.* **2021**, *71*, 166–170. [CrossRef] [PubMed]
3. Zhong, J.; Tang, J.; Ye, C.; Dong, L. The immunology of COVID-19: Is immune modulation an option for treatment? *Lancet Rheumatol.* **2020**, *2*, e428–e436. [CrossRef] [PubMed]
4. Felsenstein, S.; Herbert, J.A.; McNamara, P.S.; Hedrich, C.M. COVID-19: Immunology and treatment options. *Clin. Immunol.* **2020**, *215*, 108448. [CrossRef]
5. Shiraki, K.; Daikoku, T. Favipiravir, an anti-influenza drug against life-threatening RNA virus infections. *Pharmacol. Ther.* **2020**, *209*, 107512. [CrossRef]
6. Furuta, Y.; Komeno, T.; Nakamura, T. Favipiravir (T-705), a broad spectrum inhibitor of viral RNA polymerase. *Proc. Jpn. Acad. Ser. B Phys. Biol. Sci. P.* **2017**, *93*, 449–463. [CrossRef]
7. Imran, M.; Arora, M.K.; Asdaq, S.M.B.; Khan, S.A.; Alaqel, S.I.; Alshammari, M.K.; Alshehri, M.M.; Alshrari, A.S.; Ali, A.M.; Al-shammeri, A.M.; et al. Abida, Discovery, Development, and Patent Trends on Molnupiravir: A Prospective Oral Treatment for COVID-19. *Molecules* **2021**, *26*, 5795. [CrossRef] [PubMed]
8. Fact Sheet on Lagevrio for Healthcare Providers, Food and Drug Administration, USA. Available online: https://www.google.com/url?sa=t&rct=j&q=&esrc=s&source=web&cd=&ved=2ahUKEwjDotWU9rb5AhUihv0HHbKdD18QFnoECAMQAQ&url=https%3A%2F%2Fwww.fda.gov%2Fmedia%2F155054%2Fdownload&usg=AOvVaw3qU8nc9v1fTeeYaUUYTX8Q (accessed on 1 November 2022).
9. Toots, M.; Yoon, J.-J.; Cox, R.M.; Hart, M.; Sticher, Z.M.; Makhsous, N.; Plesker, R.; Barrena, A.H.; Reddy, P.G.; Mitchell, D.G.; et al. Characterization of orally efficacious influenza drug with high resistance barrier in ferrets and human airway epithelia. *Sci. Transl. Med.* **2019**, *11*, eaax5866. [CrossRef]
10. Rosenke, K.; Hansen, F.; Schwarz, B.; Feldmann, F.; Haddock, E.; Rosenke, R.; Barbian, K.; Meade-White, K.; Okumura, A.; Leventhal, S.; et al. Orally delivered MK-4482 inhibits SARS-CoV-2 replication in the Syrian hamster model. *Nat. Commun.* **2021**, *12*, 2295. [CrossRef]
11. Breccia, M.; Abruzzese, E.; Bocchia, M.; Bonifacio, M.; Castagnetti, F.; Fava, C.; Galimberti, S.; Gozzini, A.; Gugliotta, G.; Iurlo, A.; et al. Chronic myeloid leukemia management at the time of the COVID-19 pandemic in Italy. A campus CML survey. *Leukemia* **2020**, *34*, 2260–2261. [CrossRef]
12. Morales-Ortega, A.; Rivas-Prado, L.; Frutos-Pérez, B.; Jaenes-Barrios, B.; Farfán-Sedano, A.I.; García-Parra, C.J.; Hernández-Muniesa, B.; Duarte-Millán, M.Á.; Madroñal-Cerezo, M.E.; Ontañón-Nasarre, A.; et al. Early clinical experience with imatinib in COVID-19: Searching for a dual effect. *J. Infect.* **2021**, *82*, 186–230. [CrossRef] [PubMed]
13. Bernal-Bello, D.; Morales-Ortega, A.; Farfán-Sedano, A.I.; de Tena, J.G.; San Martín-López, J.V. Imatinib in COVID-19: Hope and caution. *Lancet* **2021**, *9*, 938–939. [CrossRef] [PubMed]
14. Report on the Deliberation Results of Avigan, Evaluation and Licensing Division, Pharmaceutical and Food Safety Bureau, Japan. 2014. Available online: https://www.google.com/url?sa=t&rct=j&q=&esrc=s&source=web&cd=&ved=2ahUKEwi5o9jB67b5AhU4g_0HHb65CkgQFnoECAMQAQ&url=https%3A%2F%2Fwww.pmda.go.jp%2Ffiles%2F000210319.pdf&usg=AOvVaw3TkoBl8Vr660a8OFm-CtE3 (accessed on 1 November 2022).
15. Product Assessment Report of Molnupiravir, European Medicines Agency, European Union. 2022. Available online: https://www.google.com/url?sa=t&rct=j&q=&esrc=s&source=web&cd=&cad=rja&uact=8&ved=2ahUKEwj4lcP16rv5AhWchv0HHcLtDW0QFnoECAIQAQ&url=https%3A%2F%2Fwww.ema.europa.eu%2Fen%2Fdocuments%2Freferral%2Flagevrio-also-known-molnupiravir-mk-4482-covid-19-article-53-procedure-assessment-report_en.pdf&usg=AOvVaw3l1W4pGFCLhRRx3AAV3n7Q (accessed on 1 November 2022).
16. Drugbank Datasheet of Molnupiravir. Available online: https://go.drugbank.com/drugs/DB15661 (accessed on 1 November 2022).
17. Datasheet of Favipiravir (CID=492405) in PubChem Database, National Institutes of Health, USA. Available online: https://www.google.com/url?sa=t&rct=j&q=&esrc=s&source=web&cd=&cad=rja&uact=8&ved=2ahUKEwjQ6J-_-sX5AhVc57sIHRyoAbsQFnoECAIQAQ&url=https%3A%2F%2Fpubchem.ncbi.nlm.nih.gov%2Fcompound%2FFavipiravir&usg=AOvVaw0n7yFNzOZ5eAh_frYbg5F6 (accessed on 1 September 2022).
18. Joshi, S.; Parkar, J.; Ansari, A.; Vora, A.; Talwar, D.; Tiwaskar, M.; Patil, S.; Barkate, H. Role of favipiravir in the treatment of COVID-19. *Int. J. Infect. Dis.* **2021**, *102*, 501–508. [CrossRef] [PubMed]
19. Siripongboonsitti, T.; Ungtrakul, T.; Watanapokasin, N.; Timsri, P.; Wongpakdee, K.; Wattanasin, P.; Pavitrapok, C.; Khunvichai, A.; Jamnongtanachot, P.; Mueannoom, W.; et al. Pharmacokinetic Comparison of Favipiravir Oral Solution and Tablet Formulations in Healthy Thai Volunteers. *Clin. Pharmacol. Drug. Dev.* **2022**, *12*, 14–20. [CrossRef] [PubMed]
20. Mentré, F.; Taburet, A.-M.; Guedj, J.; Anglaret, X.; Keïta, S.; Lamballerie, X.; Malvy, D. Dose regimen of favipiravir for Ebola virus disease. *Lancet Infect. Dis.* **2015**, *15*, 150–151. [CrossRef]
21. Du, Y.-X.; Chen, X.-P. Favipiravir: Pharmacokinetics and Concerns About Clinical Trials for 2019-nCoV Infection. *Clin. Pharmacol. Ther.* **2020**, *108*, 242–247. [CrossRef]

22. Megahed, S.M.; Habib, A.A.; Hammad, S.F.; Kamal, A.H. Experimental design approach for development of spectrofluorimetric method for determination of favipiravir; a potential therapeutic agent against COVID-19 virus: Application to spiked human plasma. *Spectrochim. Acta A Mol. Biomol. Spectrosc.* **2021**, *249*, 119241. [CrossRef]
23. Turan, Ç.; Metin, N.; Utlu, Z.; Yıldız, T.T.; Sakat, S.C. Evaluation of the frequency and intensity of favipiravir-associated yellow-green fluorescence in lunulae, hair, and face. *J. Cosmet. Dermatol.* **2022**, *21*, 1199–1207.
24. Kayıran, M.A.; Cebeci, F.; Erdemir, V.A.; Aksoy, H.; Akdeniz, N.; Gürel, M.S. Fluorescence of nails and hair on Wood's lamp examination in Covid pandemic; undefined effect of Favipiravir in humans. *Dermatol. Ther.* **2021**, *34*, e14740. [CrossRef]
25. Doran, M.A.; Aytogan, H.; Ayintap, E. Fluorescence of ocular surface in a Covid -19 patient after Favipiravir treatment: A case report. *Virol. J.* **2021**, *18*, 146. [CrossRef]
26. Fitos, I.; Visy, J.; Zsila, F.; Mády, G.; Simonyi, M. Selective binding of imatinib to the genetic variants of human α1-acid glycoprotein. *Biochim. Biophys. Acta* **2006**, *1760*, 1704–1712. [CrossRef] [PubMed]
27. Mic, M.; Pîrnău, A.; Floare, C.G.; Bogdan, M. Study of the binding affinity between imatinib and α-1 glycoprotein using nuclear spin relaxation and isothermal titration calorimetry. *Int. J. Biol. Macromol.* **2020**, *147*, 326–332. [CrossRef] [PubMed]
28. Di Muzio, E.; Polticelli, F.; Trezza, V.; Fanali, G.; Fasano, M.; Ascenzi, P. Imatinib binding to human serum albumin modulates heme association and reactivity. *Arch. Biochem. Biophys.* **2014**, *560*, 100–112. [CrossRef] [PubMed]
29. Delbaldo, C.; Chatelut, E.; Re, M.; Deroussent, A.; Seronie-Vivien, S.; Jambu, A.; Berthaud, P.; Cesne, A.L.; Blay, J.-Y.; Vassal, G. Pharmacokinetic-pharmacodynamic relationships of imatinib and its main metabolite in patients with advanced gastrointestinal stromal tumors. *Clin. Cancer. Res.* **2006**, *12*, 6073–6078. [CrossRef]
30. Beckmann, S.; Long, T.; Scheld, C.; Geyer, R.; Caffrey, C.R.; Grevelding, C.G. Serum albumin and a-1 acid glycoprotein impede the killing of Schistosoma mansoni by the tyrosine kinase inhibitor Imatinib. *Int. J. Parasitol-Drug.* **2014**, *4*, 287–295. [CrossRef]
31. Hegde, A.H.; Punith, R.; Seetharamappa, J. Optical, structural and thermodynamic studies of the association of an anti-leucamic drug imatinib mesylate with transport protein. *J. Fluoresc.* **2012**, *22*, 521–528. [CrossRef]
32. Gambacorti-Passerini, C.; Barni, R.; Coutre, P.; Zucchetti, M.; Cabrita, G.; Cleris, L.; Rossi, F.; Gianazza, E.; Brueggen, J.; Cozens, R.; et al. Role of α1 acid glycoprotein in the in vivo resistance of human BCR-ABL+ leukemic cells to the Abl inhibitor STI571. *J. Natl. Cancer Inst.* **2000**, *92*, 1641–1650. [CrossRef]
33. Gambacorti-Passerini, C.; Zucchetti, M.; Russo, D.; Frapolli, R.; Verga, M.; Bungaro, S.; Tornaghi, L.; Rossi, F.; Pioltelli, P.; Pogliani, E.; et al. α1 acid glycoprotein binds to imatinib (STI571) and substantially alters its pharmacokinetics in chronic myeloid leukemia patients. *Clin. Cancer Res.* **2003**, *9*, 625–632.
34. Hochepied, T.; Berger, F.G.; Baumann, H.; Libert, C. α1-Acid glycoprotein: An acute phase protein with inflammatory and immunomodulating properties. *Cytokine Growth Factor Rev.* **2003**, *14*, 25–34. [CrossRef]
35. Jain, S.; Gautam, V.; Naseem, S. Acute-phase proteins: As diagnostic tool. *J. Pharm. Bioallied Sci.* **2011**, *1*, 118–127. [CrossRef]
36. Bteich, M. An overview of albumin and alpha-1-acid glycoprotein main characteristics: Highlighting the roles of amino acids in binding kinetics and molecular interactions. *Heliyon* **2019**, *5*, e02879. [CrossRef] [PubMed]
37. Peters, T. *All about Albumin: Biochemistry, Genetics and Medical Applications*; Academic Press: San Diego, CA, USA, 1996.
38. Larghero, J.; Leguay, T.; Mourah, S.; Madelaine-Chambrin, I.; Taksin, A.-L.; Raffoux, E.; Bastie, J.-N.; Degos, L.; Berthaud, P.; Marolleau, J.-P.; et al. Relationship between elevated levels of α1-acid glycoprotein in chronic myelogenous leukemia in blast crisis and pharmacological resistance to imatinib (Gleevec®) in vitro and in vivo. *Biochem. Pharmacol.* **2003**, *66*, 1907–1913. [CrossRef]
39. Kretz, O.; Weiss, H.M.; Schumacher, M.M.; Gross, G. In vitro blood distribution and plasma protein binding of the tyrosine kinase inhibitor imatinib and its active metabolite, CGP74588, in rat, mouse, dog, monkey, healthy human and patients with acute lymphatic leukaemia. *Br. J. Clin. Pharmacol.* **2004**, *58*, 212–216. [CrossRef]
40. Friedman, M.L.; Schlueter, K.T.; Kirley, T.L.; Halsall, H.B. Fluorescence quenching of human orosomucoid. Accessibility to drugs and small quenching agents. *Biochem. J.* **1985**, *232*, 863–867. [CrossRef]
41. Shapiro, R.; Klein, R.S. The deamination of cytidine and cytosine by acidic buffer solutions. Mutagenic implications. *Biochemistry* **1966**, *5*, 2358–2362. [CrossRef] [PubMed]
42. Ulmann, J.; McCarthy, B.J. Alkali deamination of cytosine residues in DNA. *Biochim. Biophys. Acta* **1973**, *294*, 396–404. [CrossRef]
43. Antonov, L. Favipiravir tautomerism: A theoretical insight. *Theor. Chem. Accounts* **2020**, *139*, 145. [CrossRef] [PubMed]
44. da Silva, G. Protonation, Tautomerism, and Base Pairing of the Antiviral Favipiravir (T-705). *ChemRxiv* **2020**. [CrossRef]
45. Liang, G.; Tribolet, R.; Sigel, H. Ternary complexes in solution. 50. Dependence of intramolecular hydrophobic ligand-ligand interactions on ligand structure, geometry of the coordination sphere of the metal ion, and solvent composition. Opposing solvent effects. *Inorg. Chem.* **1988**, *27*, 2877–2887. [CrossRef]
46. Castro, B.; Pereira, J.; Gameiro, P.; Lima, J.L.F.C. Multinuclear NMR and potentiometric studies on the interaction of zinc and cadmium with cytidine and glycylglycine. The effect of the anion. *J. Inorg. Biochem.* **1992**, *45*, 53–64. [CrossRef]
47. Mohamed, M.; Shehata, M.; Shoukry, M. Trimethyltin(IV) complexes with some selected DNA constituents. *J. Coord. Chem.* **2001**, *53*, 125. [CrossRef]
48. Szakács, Z.; Béni, S.; Varga, Z.; Örfi, L.; Kéri, G.; Noszál, B. Acid-base profiling of imatinib (Gleevec) and its fragments. *J. Med. Chem.* **2005**, *48*, 249–255. [CrossRef] [PubMed]
49. Goncharov, N.V.; Belinskaia, D.A.; Shmurak, V.I.; Terpilowski, M.A.; Jenkins, R.O.; Avdonin, P.V. Serum Albumin Binding and Esterase Activity: Mechanistic Interactions with Organophosphates. *Molecules* **2017**, *22*, 1201. [CrossRef] [PubMed]

50. Li, B.; Sedlacek, M.; Manoharan, I.; Boopathy, R.; Duysen, E.G.; Masson, P.; Lockridge, O. Butyrylcholinesterase, paraoxonase, and albumin esterase, but not carboxylesterase, are present in human plasma. *Biochem. Pharmacol.* **2005**, *70*, 1673–1684. [CrossRef]
51. Fife, T.H.; Przystas, T.J. Divalent metal ion catalysis in the hydrolysis of esters of picolinic acid. Metal ion promoted hydroxide ion and water catalyzed reactions. *J. Am. Chem. Soc.* **1985**, *107*, 1041–1047. [CrossRef]
52. Zékány, L.; Nagypál, I. *Computational Methods for the Determination of Stability Constants*; Leggett, D.L., Ed.; Plenum Press: New York, NY, USA, 1985; pp. 291–353.
53. Zsila, F. Subdomain IB is the third major drug binding region of human serum albumin: Toward the three-sites model. *Mol. Pharm.* **2013**, *10*, 1668–1682. [CrossRef] [PubMed]
54. Dömötör, O.; Hartinger, C.G.; Bytzek, A.K.; Kiss, T.; Keppler, B.K.; Enyedy, É.A. Characterization of the binding sites of the anticancer ruthenium(III) complexes KP1019 and KP1339 on human serum albumin via competition studies. *J. Biol. Inorg. Chem.* **2013**, *18*, 9–17. [CrossRef]
55. Dömötör, O.; Enyedy, É.A. Binding mechanisms of half-sandwich Rh(III) and Ru(II) arene complexes on human serum albumin: A comparative study. *J. Biol. Inorg. Chem.* **2019**, *24*, 703–719. [CrossRef]
56. Yasgar, A.; Furdas, S.D.; Maloney, D.J.; Jadhav, A.; Jung, M.; Simeonov, A. High-throughput 1,536-well fluorescence polarization assays for α1-acid glycoprotein and human serum albumin binding. *PLoS ONE* **2012**, *7*, e45594. [CrossRef] [PubMed]
57. Smith, S.A.; Waters, N.J. Pharmacokinetic and pharmacodynamic considerations for drugs binding to alpha-1-acid glycoprotein. *Pharm. Res.* **2019**, *36*, 30. [CrossRef]
58. El-Gamel, S.; Wollert, U.; Müller, W.E. Optical studies on the specific interaction of dipyridamole with α1-acid glycoprotein (orosomucoid). *J. Pharm. Pharmacol.* **1982**, *34*, 152–157. [CrossRef] [PubMed]
59. Lakowicz, J.R. *Principles of Fluorescence Spectroscopy*; Springer: New York, NY, USA, 2006.
60. Browne, S.P.; Slaughter, E.A.; Couch, R.A.; Rudnic, E.M.; McLean, A.M. The influence of plasma butyrylcholinesterase concentration on the in vitro hydrolysis of cocaine in human plasma. *Biopharm. Drug Dispos.* **1998**, *19*, 309–314. [CrossRef]
61. Wang, D.; Zou, L.; Jin, Q.; Hou, J.; Ge, G.; Yang, L. Human carboxylesterases: A comprehensive review. *Acta Pharm. Sin. B* **2018**, *8*, 699–712. [CrossRef] [PubMed]
62. Jørgensen, H.G.; Elliott, M.A.; Allan, E.K.; Carr, C.E.; Holyoake, T.L.; Smith, K.D. α1-Acid glycoprotein expressed in the plasma of chronic myeloid leukemia patients does not mediate significant in vitro resistance to STI571. *Blood* **2002**, *99*, 713–715. [CrossRef]
63. Ingram, N.; Dishinger, C.; Wood, J.; Hutzler, M.; Smith, S.; Huskin, M. Effect of the plasticizer DEHP in blood collection bags on human plasma fraction unbound determination for Alpha-1-Acid Glycoprotein (AAG) binding drugs. *AAPS J.* **2019**, *21*, 5. [CrossRef]
64. Grzeskowiak, R. Extractables and Leachables in Microcentrifuge Tubes—Extensive HPLC/GC/MS Analysis. Eppendorf AG Application Note No. 417. Available online: https://www.google.com/url?sa=t&rct=j&q=&esrc=s&source=web&cd=&ved=2ahUKEwiLrIDnme_8AhWv7rsIHRztAL0QFnoECBQQAQ&url=https%3A%2F%2Fwww.eppendorf.com%2Fproduct-media%2Fdoc%2Fen%2F625557%2FConsumables_Application-Note_417_Microcentrifuge-Tubes_Extractables-Leachables-Microcentrifuge-Tubes-Extensive-HPLC-GC-MS-Analysis.pdf&usg=AOvVaw0KFoXVJAZUXAWtAYwhtJWt. (accessed on 20 January 2023).
65. Beaven, G.H.; Chen, S.-H.; D'albis, A.; Gratzer, W.B. A Spectroscopic Study of the Haemin–Human-Serum-Albumin System. *Eur. J. Biochem.* **1974**, *42*, 539–546. [CrossRef]
66. AlAjmi, M.F.; Rehman, M.T.; Khan, R.A.; Khan, M.A.; Muteeb, G.; Khan, M.S.; Noman, O.M.; Alsalme, A.; Hussain, A. Understanding the interaction between α-1-acid glycoprotein (AGP) and potential Cu/Zn metallo-drugs of benzimidazole derived organic motifs: A multi-spectroscopic and molecular docking study. *Spectrochim. Acta A Mol. Biomol. Spectrosc.* **2020**, *225*, 117457. [CrossRef]
67. Zsila, F.; Iwao, Y. The drug binding site of human α1-acid glycoprotein: Insight from induced circular dichroism and electronic absorption spectra. *Biochim. Biophys. Acta* **2007**, *1770*, 797–809. [CrossRef]
68. Luk, C.K. Study of the nature of the metal-binding sites and estimate of the distance between the metal-binding sites in transferrin using trivalent lanthanide ions as fuorescent probes. *Biochemistry* **1971**, *10*, 2838–2843. [CrossRef]
69. Enyedy, É.A.; Dömötör, O.; Varga, E.; Kiss, T.; Trondl, R.; Hartinger, C.G.; Keppler, B.K. Comparative solution equilibrium studies of anticancer gallium(III) complexes of 8-hydroxyquinoline and hydroxy(thio)pyrone ligands. *J. Inorg. Biochem.* **2012**, *117*, 189–197. [CrossRef]
70. Dömötör, O.; Aicher, S.; Schmidlehner, M.; Novak, M.S.; Roller, A.; Jakupec, M.A.; Kandioller, W.; Hartinger, C.G.; Keppler, B.K.; Enyedy, É.A. Antitumor pentamethylcyclopentadienyl rhodium complexes of maltol and allomaltol: Synthesis, solution speciation and bioactivity. *J. Inorg. Biochem.* **2014**, *134*, 57–65. [CrossRef]
71. Gans, P.; Sabatini, A.; Vacca, A. Investigation of equilibria in solution. Determination of equilibrium constants with the HYPERQUAD suite of programs. *Talanta* **1996**, *43*, 1739–1753. [CrossRef]
72. Irving, H.M.; Miles, M.G.; Pettit, L.D. A study of some problems in determining the stoicheiometric proton dissociation constants of complexes by potentiometric titrations using a glass electrode. *Anal. Chim. Acta* **1967**, *38*, 475–488. [CrossRef]
73. SCQuery. *The IUPAC Stability Constants Database, Academic Software, Version 5.5*; Royal Society of Chemistry: London, UK, 1993.
74. Żołek, T.; Dömötör, O.; Ostrowska, K.; Enyedy, É.A.; Maciejewska, D. Evaluation of blood-brain barrier penetration and examination of binding to human serum albumin of 7-O-arylpiperazinylcoumarins as potential antipsychotic agents. *Bioorganic Chem.* **2019**, *84*, 211–225. [CrossRef]

75. Enyedy, É.A.; Dömötör, O.; Bali, K.; Hetényi, A.; Tuccinardi, T.; Keppler, B.K. Interaction of the anticancer gallium(III) complexes of 8-hydroxyquinoline and maltol with human serum proteins. *J. Biol. Inorg. Chem.* **2015**, *20*, 77–88. [CrossRef]
76. Puigdomenech, I. Making Equilibrium Diagrams Using Sophisticated Algorithms (MEDUSA). Available online: https://www.kth.se/che/medusa/ (accessed on 20 January 2023).